UNIVERSIDADE ESTADUAL DE GOIÁS
CAMPUS DE CIÊNCIAS EXATAS E TECNOLÓGICAS
PROGRAMA DE PÓS-GRADUAÇÃO STRICTO SENSU EM CIÊNCIAS MOLECULARES

DESCRIÇÃO ISOESTRUTURAL DE DUAS CHALCONAS HALOGENADAS

GABRIELA SILVA LUDOVICO

Anápolis, GO
2021

GABRIELA SILVA LUDOVICO

DESCRIÇÃO ISOESTRUTURAL DE DUAS CHALCONAS HALOGENADAS

Dissertação de mestrado apresentada ao Programa de Pós-Graduação *Stricto Sensu* em Ciências Moleculares, da Universidade Estadual de Goiás, como parte dos requisitos para obtenção do título de Mestre em Ciências Moleculares.

Área de concentração: Análise Estrutural de Compostos Químicos e Fármacos

Orientador: Prof. Dr. Hamilton Barbosa Napolitano

Anápolis, GO
2021

TERMO DE AUTORIZAÇÃO PARA PUBLICAÇÃO DE TESES E DISSERTAÇÕES NA BIBLIOTECA DIGITAL (BDTD)

Na qualidade de titular dos direitos de autor, autorizo a Universidade Estadual de Goiás a disponibilizar, gratuitamente, por meio da Biblioteca Digital de Teses e Dissertações (BDTD/UEG), regulamentada pela Resolução, **CsA n.1087/2019** sem ressarcimento dos direitos autorais, de acordo com a Lei nº 9610/98, o documento conforme permissões assinaladas abaixo, para fins de leitura, impressão e/ou *download*, a título de divulgação da produção científica brasileira, a partir desta data.

Dados do autor (a)

Nome Completo: Gabriela Silva Ludovico

E-mail: ludovicogabrielasilva@gmail.com

Dados do trabalho

Título: Descrição Isoestrutural de Duas Chalconas Halogenadas

Data da Defesa: 03 / 03 / 2021

Tipo

( ) Tese (X) Dissertação

Programa de Mestrado em Ciências Moleculares

Concorda com a liberação documento

[X] SIM

[ ] NÃO **Casos de impedimento:** Período de embargo por até um ano a partir da data de defesa. A extensão deste prazo necessita de justificativa junto à coordenação do curso.

- [ ] Solicitação de registro de patente;
- [ ] Submissão de artigo em revista científica;
- [ ] Publicação como capítulo de livro;
- [ ] Publicação da dissertação/tese em livro.

Anápolis, 15/ 03 / 2021

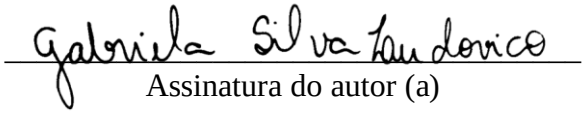

Assinatura do autor (a)

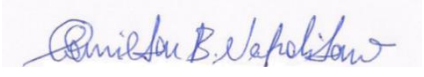

Assinatura do orientador (a)

Elaborada pelo Sistema de Geração Automática de Ficha Catalográfica da UEG
com os dados fornecidos pelo(a) autor(a).

Ld Ludovico, Gabriela Silva
Descrição Isoestrutural de Duas Chalconas Halogenadas / Gabriela Silva Ludovico; orientador Hamilton Barbosa Napolitano. -- Anápolis, 2021.
56 p.

Dissertação (Mestrado - Programa de Pós-Graduação Mestrado Acadêmico em Ciências Moleculares) -- Câmpus Central - Sede: Anápolis - CET, Universidade Estadual de Goiás, 2021.

1. Cristalografia. 2. Chalconas. 3. Isoestruturas. I. Napolitano, Hamilton Barbosa , orient. II. Título.

DESCRIÇÃO ISOESTRUTURAL DE DUAS CHALCONAS HALOGENADAS

GABRIELA SILVA LUDOVICO

Dissertação apresentada ao Programa de Mestrado em Ciências Moleculares do Campus Anápolis de Ciências Exatas e Tecnológicas Henrique Santillo, da Universidade Estadual de Goiás, apresentada como parte dos requisitos necessários para obtenção do título de Mestre em Ciências Moleculares.

Aprovada em 3/03/2021 por:

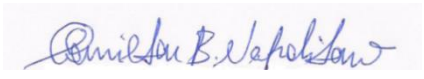

Prof. Dr. Hamilton Barbosa Napolitano (Orientador/UEG)

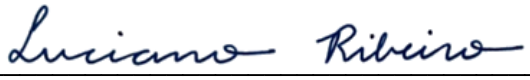

Prof. Dr. Luciano Ribeiro (UEG)

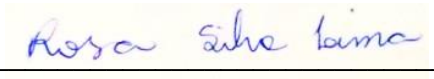

Profa. Dra. Rosa Silva Lima (Faculdade Fibra)

ANÁPOLIS – GO

AGRADECIMENTOS

A Deus, que me capacitou em sabedoria para realizar esta tarefa.

Aos meus familiares, pelo apoio e incentivo sempre manifestos em auxílios e toda sorte de ajuda em todas as etapas da minha vida.

Ao meu orientador, professor Hamilton, pela amizade, paciência, apoio e por todo conhecimento que me transmitiu com sabedoria.

Aos meus amigos que me ajudaram a chegar até aqui.

Aos professores e colegas do Programa de Pós Graduação em Ciências Moleculares que sempre estiveram dispostos a ajudar e ensinar colaborando com meu desenvolvimento acadêmico.

Ao Instituto de Física de São Carlos, pela participação no Programa de Pesquisa para Estudantes Visitantes, do Programa de Pós Graduação em Física.

Aos professores e organizadores do *ACA Summer Course in Chemical Crystallography* e ao International Centre for Diffraction Data pelo suporte acadêmico para participação neste curso.

Ao professor Dr. Allen Oliver e ao Dr. Jean Custodio, pela coleta dos dados de difração de raios-X, e por me receberem no laboratório de *Molecular Structure Facility*, do Departamento de Química e Bioquímica da *University of Notre Dame.*

À Coordenação de Aperfeiçoamento de Pessoal de Nível Superior (CAPES), pela bolsa de estudos, que me permitiu me dedicar integralmente ao mestrado.

“Aos que me apoiaram durante esta jornada de aprendizado e crescimento.”

RESUMO

As chalconas são um importante grupo de compostos orgânicos que têm despertado grande interesse científico devido às diversas propriedades que possuem e podem apresentar variados potenciais biológicos, além das propriedades ópticas. A cristalografia é uma metodologia científica que permite a elucidação estrutural de compostos químicos para estudar suas propriedades, a qual considera a relação existente entre a estrutura e as propriedades das moléculas. Este trabalho determinou a estrutura de um novo derivado de chalcona cloro substituída em comparação com uma chalcona bromo substituída descrito na literatura, esta comparação permitiu o entendimento da influência dos halogênios como substituintes nas chalconas. Neste estudo, métodos cristalográficos foram utilizados para elucidar a estrutura cristalina das chalconas, analisar os parâmetros geométricos e do arranjo supramolecular das chalconas e mostrar que a substituição de um halogênio por outro não causa grandes alterações estruturais. As moléculas deste estudo mostraram-se ser isoestruturas, ou seja, têm estruturas moleculares muito semelhantes.

Palavras – chave: Cristalografia; Chalcona; Halogênios; Isoestrutura.

ABSTRACT

Chalcones are an important group of organic compounds which have aroused great scientific interest due to the diverse properties they possess, may have varied biological potentials in addition to optical properties. Crystallography is a scientific methodology that allows the structural elucidation of chemical compounds to study their properties, taking into account the existing relationship between the structure and the properties of molecules this work determined the structure of a new chalcone derivative chlorine substituted in compared with a chalcone bromo substituted described in the literature, this comparison allowed the understanding of the influence of halogens as substituents in chalcones. In this study, crystallographic methods were used to elucidate the crystal structure of chalcones, the analysis of geometric parameters and supramolecular arrangement of chalcones shows that the substitution of one halogen for another does not cause major structural changes, the molecules of this study were shown to be isostructures, that is, have very similar molecular structure.

Key – words: Crystallography; Chalcone; Halogens; Isostructure.

LISTA DE ILUSTRAÇÕES

SUMÁRIO

1 INTRODUÇÃO

Nos últimos anos, tem-se crescido muito a busca pelo desenvolvimento de novos compostos com potenciais aplicações farmacológicas e também tecnológicas (GUIDO; ANDRICOPULO; OLIVA, 2010). A cristalografia fornece dados das posições dos átomos na molécula, ou seja, a estrutura molecular tridimensional. O conhecimento dessa estrutura molecular é muito relevantes na obtenção de informações referentes às propriedades dos compostos químicos (devido à relação estrutura propriedade), essas informações possuem diversas utilidades como na pesquisa de fármacos, no estudo de moléculas biológicas e no desenvolvimento de materiais (ALMEIDA et al., 2014).

As chalconas e seus derivados são um importante grupo de moléculas que tomou destaque em estudos devido as suas diversas atividades biológicas, quais sejam anti-inflamatórias, antifúngicas, anticâncer, antioxidante, antibiótico e antidiabético (ABU et al., 2013; HSIEH et al., 2012; NOWAKOWSKA, 2007; OSORIO et al., 2018; WON et al., 2005). E podem também apresentar propriedades ópticas. Em regra, todas essas propriedades estão relacionadas com os substituintes ligados nos anéis A e B (DUARTE et al., 2019).

Figura 1- Estrutura geral das chalconas

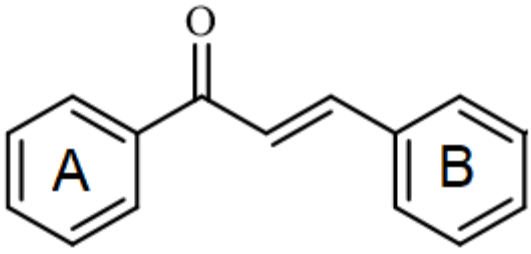

Esse grupo de moléculas são formados por dois anéis aromáticos ligados por um grupamento carbonil α, β insaturado (Figura 1), esse sistema π-conjugado gera uma deslocalização da nuvem eletrônica em torno de todo o composto. São derivados de produtos naturais e podem ser também obtidos por via sintética, o que

permite a incorporação de diversos grupos funcionais em seus anéis (KUSZ; MAŁECKA; CHE, 2020; ZAINURI; RAZAK; ARSHAD, 2018)

Este trabalho tem como objetivo empregar a metodologia cristalográfica para estudar como a troca do substituinte cloro por bromo influencia a estrutura molecular, o empacotamento, as interações e o arranjo supramolecular em uma chalcona. As chalconas empregadas neste trabalho são a 3- (3-chlorophenyl) -1-phenylprop-2-en-1-one (CLC) e a 3- (3-bromophenyl) -1-phenylprop-2-en-1-one (BRC).

A amostra do composto CLC foi sintetizado e cristalizado pela professora Dra. Rosa S. Lima (Faculdade do Instituto Brasil de Ciência e Tecnologia) e o cristal obtido foi coletado e resolvido. Os dados do composto BRC foram retirados do banco de dados do CCDC, as informações obtidas foram analisadas através da comparação das interações presentes, das distâncias de ligação, do empacotamento e do arranjo supramolecular. Para se obter as informações necessárias sobre as moléculas, foram utilizados de programas computacionais, qual seja, a plataforma OLEX2 que foi utilizada para resolver e visualizar as estruturas, bem como, os programas Mercury e CrystalExplorer que foram utilizados para analisar o empacotamento, as interações e o arranjo supramolecular.

2 TÓPICOS DE CRISTALOGRAFIA

A determinação da estrutura molecular dos compostos químicos é indispensável para conhecer suas propriedades físico-químicas e biológicas e assim determinar uma aplicação para esse composto, entretanto, essa determinação não é simples. Existem diversas metodologias para determinação da composição molecular de um produto, porém, a maioria dessas organizações parte de um princípio comparativo, enquanto a cristalografia é uma metodologia *ab initio* que determina a estrutura molecular de um cristal através do fenômeno da difração de raios X, (ALMEIDA *et al*., 2014; DRENTH, 1994).

A determinação da estrutura molecular de um composto é dada pela interação entre a radiação e o composto no estado cristalino. Essa radiação interage com os elétrons presentes no composto de acordo com a distribuição espacial desses elétrons. Processando-se, computacionalmente, os dados obtidos da difração de raios X, é possível obter a densidade eletrônica e determinar o arranjo tridimensional dos átomos, e desse modo, estudar as interações atômicas e os ângulos de ligação. Ademais, as informações do conteúdo cristalino a nível atômico são importantes para o entendimento das propriedades da molécula (BLAKE et al., 2009), em que é necessário, primeiramente, conhecer os conceitos envolvidos (GLUSKER; LEWIS; ROSSI, 1994).

2.1 SIMETRIA

Um cristal é um sólido composto por uma grande quantidade de moléculas idênticas posicionadas em um padrão regular e com periodicidade tridimensional em uma área delimitada chamada célula unitária (VENCATO, 1988). As operações de simetria permitem a reprodução do cristal por meio da repetição de uma base molecular. As operações de simetria tornam o sistema invariante e são empregadas no estudo de estruturas moleculares por entre os elementos de simetria. Contanto, um elemento de simetria é uma entidade geométrica onde a operação de simetria tem como referencial um eixo, um ponto, um plano e um vetor, alguns exemplos de

elementos de simetria são a rotação, inversão e translação (GLUSKER; TRUEBLOOD, 2010).

A cela unitária (Figura 2) é uma unidade de repetição equivalente que se repete por translação na estrutura cristalina e pode ser definido como um elemento de volume. É um paralelepípedo caracterizado por seis parâmetros, divididos em axiais (**a, b, c**) e angulares (α, β, γ). As faces da cela unitária contem pares de vetores **b** e **c** , **c** e **a** , e **a** e **b** são respectivamente as faces A, B e C da cela z**.**

Figura 2**-** Representação tridimensional de uma cela unitária

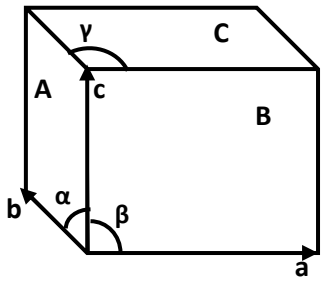

Fonte: Adaptado (GIACOVAZZO et al., 2011).

Considerando-se os parâmetros de cela unitária, podemos classificar os cristais em sete sistemas cristalinos: triclínico (a ≠ b ≠ c e α ≠ β ≠ γ), monoclínico (a ≠ b ≠ c e α = γ ≠ β), ortorrômbico (a ≠ b ≠ c e α = β = γ = 90º), tetragonal (a = b ≠ c e α = β = γ = 90º), trigonal e hexagonal (a = b = c e α = β = 90º ≠ γ), e cúbico (a = b = c e α = β = γ = 90º) (GIACOVAZZO et al., 2011).

Em vista das possíveis localizações das partículas na cela unitária, tem-se a seguinte caracterização: rede Primitiva, P, onde todos os pontos estão localizados nos vértices da cela unitária; rede de face centrada nas faces A, B ou C, apresentando pontos nas faces além daqueles localizados nos vértices; rede de corpo centrado, I, onde, além dos pontos que determinam os vértices, possui um ponto reticular no centro da cela e rede com todas as faces centradas, F. Ademais, com a combinação dos sete sistemas cristalinos e a centragem da cela, temos as quatorze redes cristalinas denominadas redes de Bravais (Figura 3) (GIACOVAZZO et al., 2011; GLUSKER; LEWIS; ROSSI, 1994).

Figura 3- Representação tridimensional das 14 redes de Bravais

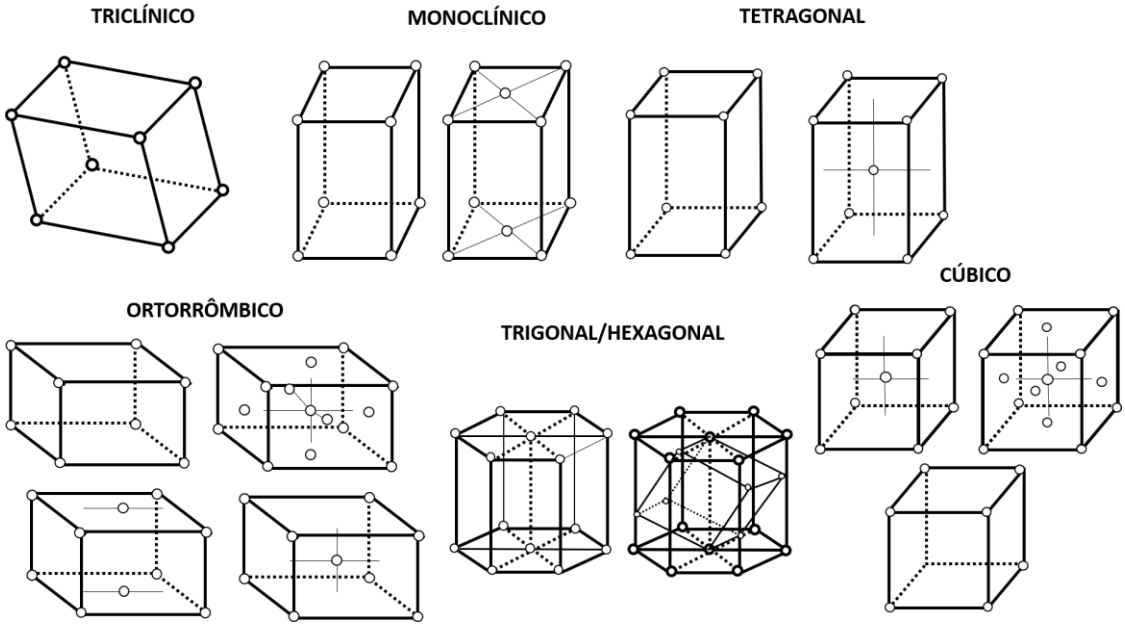

Fonte: Adaptado (GIACOVAZZO et al., 2011).

Os sistemas cristalinos não são determinados pelos seus parâmetros de cela unitária (**a**, **b**, **c**, α, β, γ), mas pela operação de simetria neles existente, definida pelo grupo pontual. A simetria pontual descreve a repetição periódica em torno de um ponto. Um grupo pontual é um conjunto de todas as operações de simetria para uma molécula, as operações de simetria possíveis são classificadas em próprias e impróprias, as quais rotações de uma determinada fração de 360° em torno de um eixo de rotação são reconhecidas como próprias, já o espelho e o centro de inversão são entendidos como elementos de simetria impróprios, que alteram a quiralidade e causam uma mudança da conectividade da estrutura, cada grupo pontual possui sua própria característica e um símbolo convencional (BLAKE et al., 2009; GIACOVAZZO et al., 2011).

Os cristais podem ser classificados em grupos a partir da combinação entre suas operações de simetria (dos eixos de rotação próprios e impróprios). Esses grupos formados são conhecidos como os 32 grupos pontuais e existe uma combinação possível dos elementos de simetria cristalográficos, respeitadas as suas restrições quanto às combinações, uma vez que a combinação de duas operações de simetria necessariamente criará uma terceira operação. Desse modo, combinando os 32 grupos pontuais com as 14 redes de Bravais, temos os 230 grupos espaciais (GIACOVAZZO et al., 2011; GLUSKER; LEWIS; ROSSI, 1994).

2.2 DIFRAÇÃO DE RAIOS X

A difração é um fenômeno ondulatório, verificada quando um feixe de fótons incide sobre um obstáculo que contém um ou mais orifícios com dimensões da ordem de seu comprimento de onda. A difração de raios X é o processo de espalhamento que ocorre quando o campo elétrico da radiação interage com a matéria. Os raios X são radiações cujo comprimento de onda é da ordem de 0,1 a 100 Å, o que é muito pequeno em comparação ao do espectro visível. Quando um feixe de raios X incide em um cristal em condições geométricas adequadas, este é espalhado pela nuvem eletrônica dos átomos, as cargas elétricas dos átomos são aceleradas pelo campo elétrico e emitem radiação em todas as direções (NAPOLITANO et al., 2007; VENCATO, 1988).

Como a amostra cristalina possui vários espaços vazios, mais de 98% do feixe de raios X passa diretamente pela amostra. Ao colidirem com o átomo, os raios X promovem a oscilação dos elétrons em torno do núcleo, e ao vibrarem emitem radiação, a análise das emissões de dois elétrons mostra que as radiações emitidas formam ondas que se superpõem. Essa superposição das ondas é denominada interferência. Devido à simetria presente nos cristais, a interferência obedece a regularidades que geram a interferência construtiva. A interação dos raios X com estruturas cristalinas constitui uma ferramenta extremamente útil, precisa e aplicável na determinação estrutural de diversos compostos (CHATTERJEE, 2008; GLUSKER; TRUEBLOOD, 2010).

Figura 4- Reflexão do raio X por dois planos consecutivos

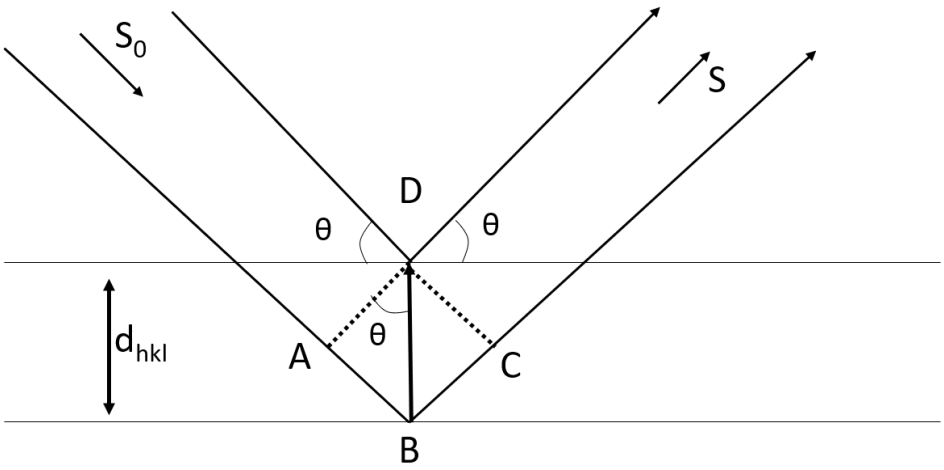

Fonte: Adaptado (GIACOVAZZO et al., 2011).

A difração de raios X pelos átomos das estruturas cristalinas gera um padrão de difração cuja análise fornece as características estruturais especificas da substância analisada. A condição para que se observe a difração de um feixe de raios X pelo cristal é dada pela Lei de Bragg, descrita na equação 1 (CULLITY, 2001; VLACK, 1970)

$$n\lambda = 2\, d_{hkl}\, \mathrm{sen}\theta\ , \qquad (1)$$

em que n é um número inteiro, d é a distância entre planos paralelos, λ é o comprimento de onda dos raios X e θ é o ângulo de incidência. A Figura 4 e a Equação 1 mostram que a lei de Bragg é uma consequência da periodicidade da rede cristalina e estabelece uma condição que determina que a diferença de caminho óptico seja um múltiplo inteiro do comprimento de onda do feixe incidente (STOUT; JENSEN, 1989; VLACK, 1970).

2.3 DENSIDADE ELETRÔNICA E O PROBLEMA DA FASE

Levando-se em consideração a densidade eletrônica de um único átomo, com o seu centro coincidente com a origem do sistema de coordenadas da cela unitária, a amplitude da onda espalhada por esse átomo será igual ao fator espalhamento atômico conforme a Equação 2 (STOUT; JENSEN, 1989):

$$f_j = \rho(r_j) e^{2\pi i r_j \cdot S}, \qquad (2)$$

onde f_j é o fator de espalhamento atômico do átomo. O espalhamento a partir de uma região com densidade eletrônica $\rho(r)$ pode ser expresso pelo Fator de Estrutura F(S).

O fator de estrutura é o efeito do espalhamento das ondas nas direções hkl, por todos os átomos da cela. O fator de estrutura F(S), será a soma vetorial das contribuições dos N átomos da cela unitária, conforme a Eq. (3) expressa para uma única cela unitária :

$$F(hkl) = \sum_{j-1}^{N} f_j\ e^{2\pi i(hx_j + ky_j + lz_j)}. \qquad (3)$$

O fator de estrutura é um número complexo que representa o espalhamento de raios X por todos os componentes da cela unitária, e oferece uma descrição matemática do padrão de difração. Conhecendo-se as posições de todos os átomos na cela, podemos calcular o correspondente padrão de difração, o padrão de difração

$F_{(S)}$ está relacionado com a densidade eletrônica $\rho(r)$ pela operação matemática da transformada de Fourier (ALMEIDA et al., 2014).

Desenvolvida por Baron Jean Baptiste Fourier, este teorema estabelece que qualquer função de uma variável contínua pode ser expressa em uma série de harmônicos de senos e cossenos. Assim, o fator de estrutura é a análise de Fourier da estrutura cristalina, já a densidade eletrônica é a síntese de Fourier, a Equação 4 relaciona o fator de estrutura e a densidade eletrônica. O experimento da difração de raio X fornece dados do padrão de difração, as amplitudes por medidas diretas das intensidades, contudo, os dados referentes às fases não podem ser coletados (BLAKE et al., 2009).

$$\rho(xyz) = \frac{1}{V}\sum_{hkl} F_{hkl}\, e^{-2\pi i(hx+ky+lz)+i\varphi}. \quad (4)$$

Como as fases relativas das ondas espalhadas são perdidas durante o experimento, não é possível calcular a densidade eletrônica ρ pela equação 4, pois os valores de φ são desconhecidos, esse problema é conhecido como problema da fase. Para solucionar o problema da fase em cristalografia de pequenas moléculas, emprega-se os métodos diretos, uma metodologia que possibilita encontrar as fases do Fator de Estrutura F(S) através de relações matemáticas a partir de um simples conjunto de intensidades medidas experimentalmente, tornando-se, dessa maneira, possível calcular a densidade eletrônica $\rho(r)$ para cada posição r da cela unitária através da Equação 4 (ALMEIDA et al., 2014; GIACOVAZZO et al., 2011).

2.4 COLETA DE DADOS, SOLUÇÃO DA ESTRUTURA E REFINAMENTO

Os dados obtidos do experimento de difração de raios X, consistem nas intensidades e nas posições dos feixes difratados. A coleta de dados consiste no procedimento de medida das intensidades das ondas difratadas, das quais se obtém um conjunto de imagens que são integradas e processadas. Resulta-se, desse modo, um conjunto de reflexões que fornece tanto a direção hkl quanto a intensidade de cada feixe difratado (BLAKE et al., 2009).

Ao verificar os parâmetros da cela unitária, o seu conteúdo e a simetria do cristal, é possível resolver a estrutura utilizando programas computacionais que

empregam os métodos estatísticos. A estrutura é resolvida a partir da determinação das fases de cada reflexão através dos métodos diretos, calculando, portanto, a densidade eletrônica da cela (GIACOVAZZO et al., 2011).

Para resolver a estrutura, utiliza-se de programas computacionais SHELXS 97 e/ou SIR, de programas WingGX, ou mesmo, Olex. A partir da resolução das estruturas, obtém-se os mapas de densidade eletrônica. Calculados a partir dos melhores conjuntos de fases, os mapas são obtidos pela síntese de Fourier, usa-se coeficientes da série os fatores de estrutura normalizados. A partir do mapa de densidade eletrônica, inicia-se a determinação da estrutura através da interpretação dos mapas obtendo as posições aproximadas dos átomos (ALMEIDA et al., 2014).

Figura 5**-** Representação da construção de um mapa de densidade eletrônica

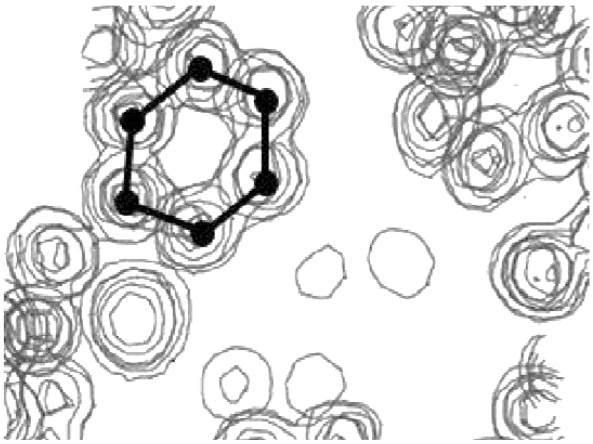

Fonte: (ALMEIDA et al., 2014).

O refinamento é o procedimento de minimização da discordância entre os módulos dos fatores de estrutura observado e calculado, que realiza pequenas modificações nos parâmetros atômicos determinados, portanto, das fases calculadas, para a estrutura aproximada. Uma vez obtida a estrutura molecular aproximada, as posições atômicas deverão ser refinadas pelo uso da técnica dos mínimos quadrados até obter a melhor convergência entre os dados de intensidade observados e os calculados de acordo com o modelo da estrutura preliminar. Os mínimos quadrados são princípios, em que a soma dos erros ao quadrado é minimizada por meio da função M, descrita pela Equação 5 (GLUSKER; TRUEBLOOD, 2010; MÜLLER et al., 2006):

$$M = \sum_{hkl} w_h \left[|F(h)|^2_{obs} - |F(h)|^2_{cal}\right]^2, \quad (5)$$

cujo w é o peso atribuído a cada reflexão, uma vez que o melhor modelo é aquele que minimiza M.

Por fim, concluído o processo de construção do modelo estrutural de um composto, todas as informações cristalográficas devem ser armazenadas em um arquivo-texto comum, de acordo com o padrão *Crystallographic Information File* (CIF), estabelecido pela *International Union of Crystallography* (IUCR) (ALMEIDA et al., 2014; STOUT; JENSEN, 1989).

Para validar o modelo estrutural, a início, é necessário analisar os possíveis erros e garantir a veracidade dos resultados das estruturas resolvidas. Existem dois tipos de erros: os sistemáticos, esses são identificados e corrigidos, e os randômicos, que, por sua vez, não podem ser corrigidos, pois ocorrem em variáveis não controláveis. A qualidade de uma estrutura cristalográfica pode ser obtida pela comparação entre os fatores medidos experimentalmente e fatores calculados. Esses índices são avaliados estatisticamente pelas Figuras de Mérito, que são o *Goodness of Fit* (GOOF), que é o grau com que a distribuição das diferenças entre os conjuntos se ajusta aos valores esperados, afetados pelos erros randômicos, e o Índice de discordância, *R*, esse compreende ao grau de precisão do modelo cristalográfico construído (GIACOVAZZO et al., 2011; MÜLLER et al., 2006).

3 RESULTADOS E DISCUSSÕES

Esse trabalho realizou o estudo comparativo de duas chalconas (uma inédita e outra retirada do banco de dados do CCDC), com o intuito de compreender como a substituição dos halogênios cloro por bromo influenciam na estrutura molecular da chalcona. Também foram realizados estudos das propriedades ópticas não lineares e cálculos de mecânica quântica em colaboração com o Prof. Dr. Clodoaldo Valverde (Universidade Estadual de Goiás) e com o Prof. Dr. Ademir J. Camargo (Universidade Estadual de Goiás).

3.1 CARACTERIZAÇÃO CRISTALOGRÁFICA

As moléculas de CLC e BRC cristalizaram no sistema cristalino monoclínico, no grupo espacial $P2_1/c$, os dados de coleta e refinamento estão presentes na Tabela 1.

Tabela 1. Dados de coleta e refinamento para as moléculas de CLC e BRC.

Crystal data	**CLC**	**BRC**
Chemical formula	$C_{15}H_{11}ClO$	$C_{15}H_{11}BrO$
M_r	242.69	287.15
Crystal system, space group	$P2_1/_C$	$P2_1/_C$
Temperature (K)	296	100
a, *b*, *c* (Å)	14.100(3), 7.4948(16), 11.230(3)	14.3238(2), 7.4913(1), 11.2786(2)
α, β, γ (°)	90, 101.009(4), 90	90, 100.325(1), 90
V (Å^3)	1164.9(5)	1190.64(3)
Z	4	4
μ (mm^{-1})	0.306	3.43
$R[F^2 > 2\sigma(F^2)]$	0.0428	0.030
S	1.026	1.10
No. of reflections	2852	7339
No. of parameters	154	154

As estruturas moleculares das chalconas estudadas estão representadas na Figura 6, consistem em chalconas simples como mostrado na Figura 1 com um substituinte na posição meta ligado ao anel B da chalcona, cloro na molécula de CLC (Figura 6a) e um substituinte bromo na molécula BRC (figura 6b).

Figura 6- Representação Ortep com 75% de probabilidade para as moléculas de (a) CLC e (b) BRC

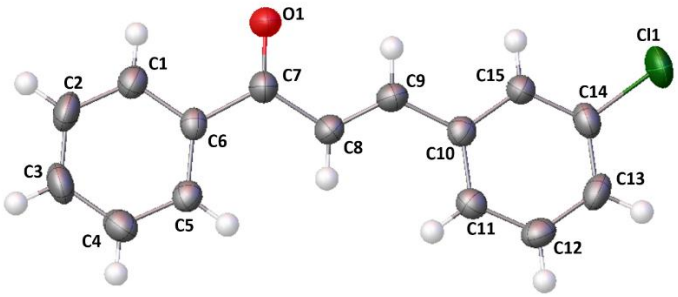

(a)

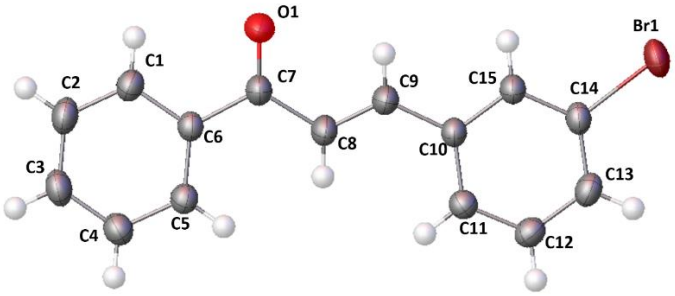

(b)

As interações intramoleculares e intermoleculares presentes são do tipo CH ... O (Figura 7), C-H ... Cl (Figura 8 a), C-H ... Br (Figura 8 b), C-H ... H-C (Figura 9), C-H … π e π… π todas essas interações mantem o arranjo cristalino, a Tabela 2 mostra as interações e as distâncias de ligação.

Figura 7- Arranjo molecular para mostrar interações C–H…O para CLC (a) e BRC (b)

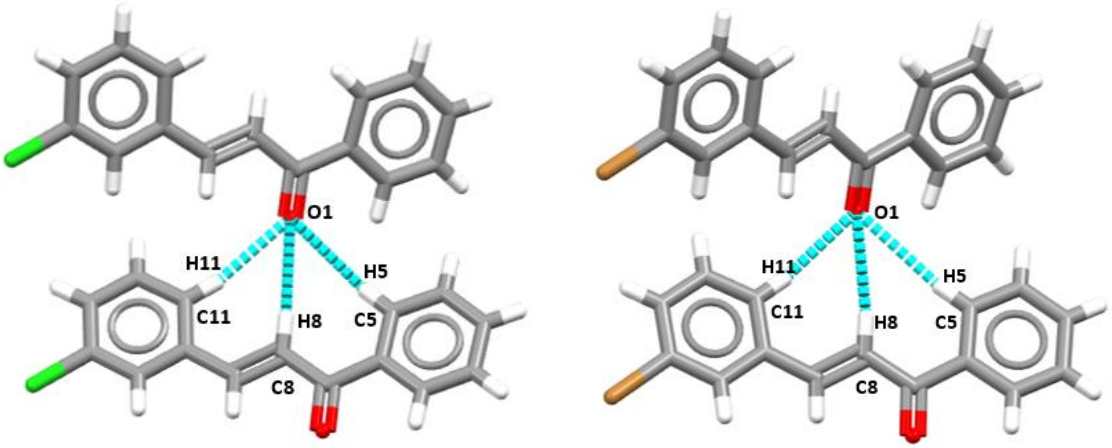

(a) (b)

Figura 8- Arranjo molecular para mostrar interações (a) C–H…Cl para CLC e (b) C–H…Br para molécula BRC

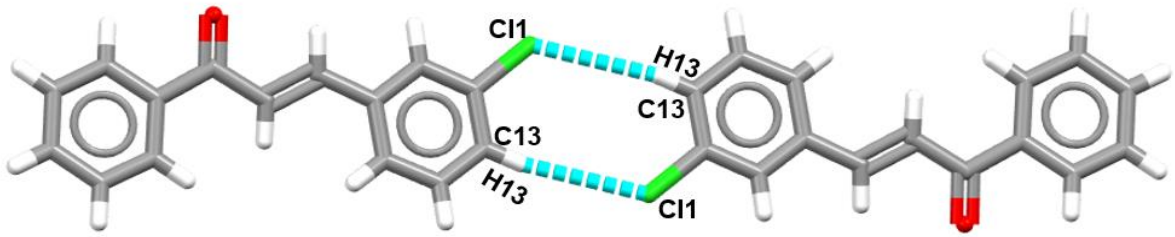

(a)

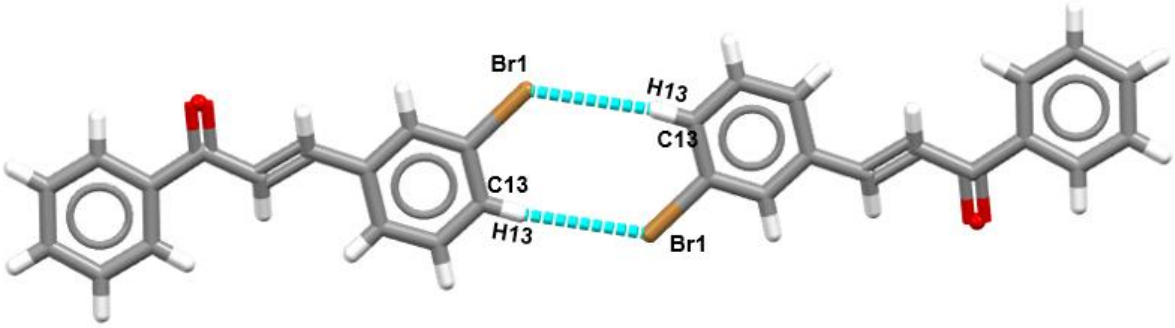

(b)

Figura 9- Arranjo molecular para mostrar interações C–H…H–C para (a) CLC e (b) BRC

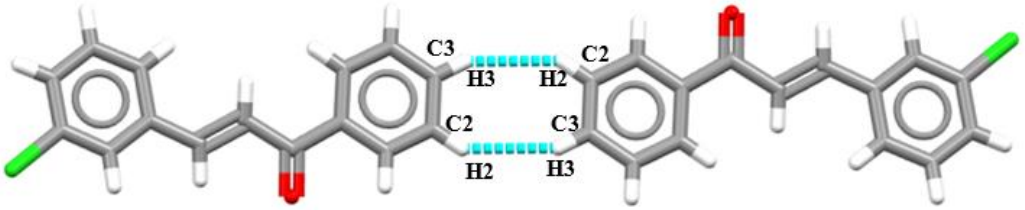

(a)

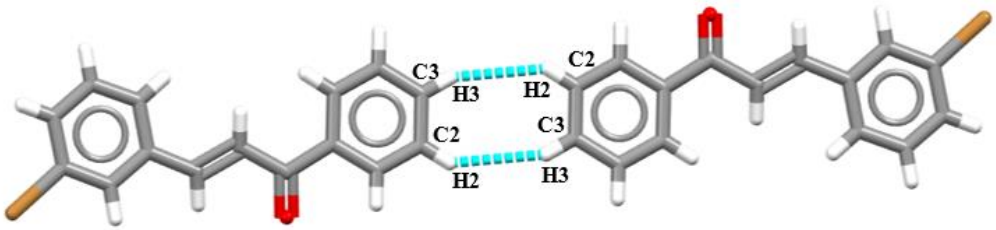

(b)

Table 2. Hydrogen-bond geometry (Å, °) for CLC and BRC.

	D – H···A	**D – H**	**H···A**	**D···A**	**D – H···A**	**Symmetry code**
CLC	C11–H11···O1	0.93	2.49	3.399	165	x,1/2-y,1/2+z
	C13–H13···Cl1	0.93	2.99	3.905	167	-x,-y,1-z
	C5–H5···O1	0.93	2.49	3.399	164	x,1/2-y,1/2+z
	C8–H8···O1	0.93	2.78	3.684	166	x,1/2-y,1/2+z
	C2–H2···H3–C3	0.93	2.51	4.111	146	2-x,1-y,1-z
	C3–H3···H2–C2	0.93	2.51	4.111	154	2-x,1-y,1-z
BRC	C11–H11···O1	0.93	2.50	3.411	166	x,1/2-y,1/2+z
	C13–H13···Br1	0.93	3.09	4.000	164	-x,-y,1-z
	C5–H5···O1	0.93	2.79	3.717	172	x,1/2-y,1/2+z
	C8–H8···O1	0.93	2.79	3.700	165	x,1/2-y,1/2+z
	C2–H2···H3–C3	0.93	2.62	4.221	143	2-x,1-y,1-z
	C3–H3···H2–C2	0.93	2.62	4.221	155	2-x,1-y,1-z

As interações encontradas na molécula CLC também foram encontradas na molécula BRC, com pequenas diferenças nas distâncias de ligação, como mostrado nos dados da Tabela 2, a sobreposição das moléculas (Figura 10) e o empacotamento molecular (Figura 11) mostram que a troca dos substituintes cloro/bromo não provocou alteração na estrutura molecular.

Figura 10- Sobreposição das estruturas moleculares CLC (verde) e BRC (marrom)

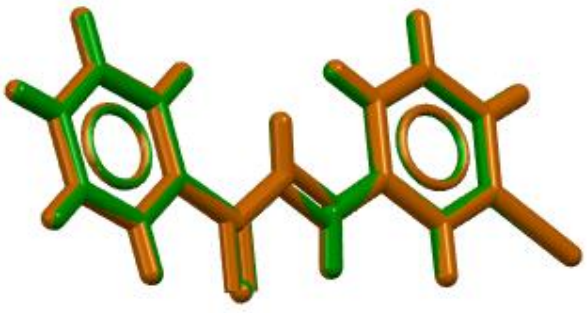

Figura 11- Empacotamento cristalino (a) para a molécula de CLC, (b) para a molécula de BRC

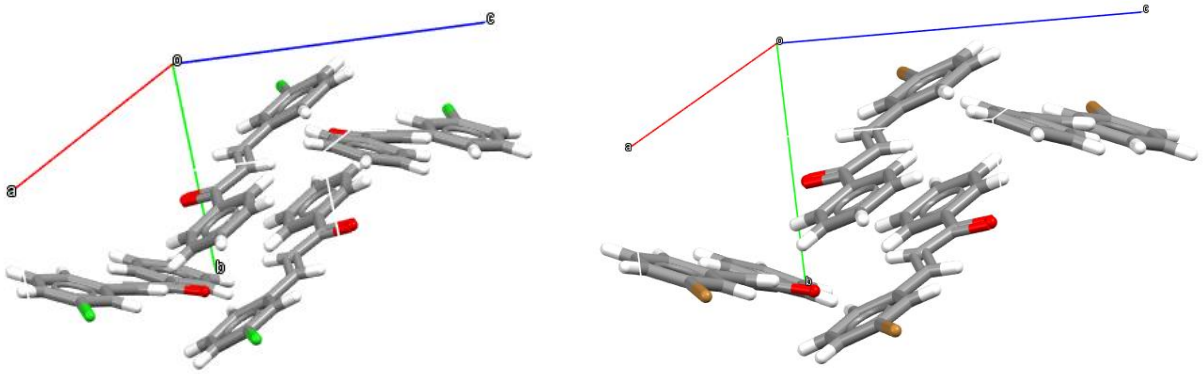

(a) (b)

A Superfície de Hirshfeld d_{norm} (Figura 12) as interações H...O presentes nas moléculas, a área azul da superfície representa a ausência de interações e os pontos vermelhos são as áreas com interações, a Figura 12 (a) mostra a interação C11-H11...O1 para o CLC e a Figura 12 (b) a interação C11-H11...O1 para o BRC.

Figura 12- Superfície de Hirshfeld dnorm (a) CLC e (b) BRC

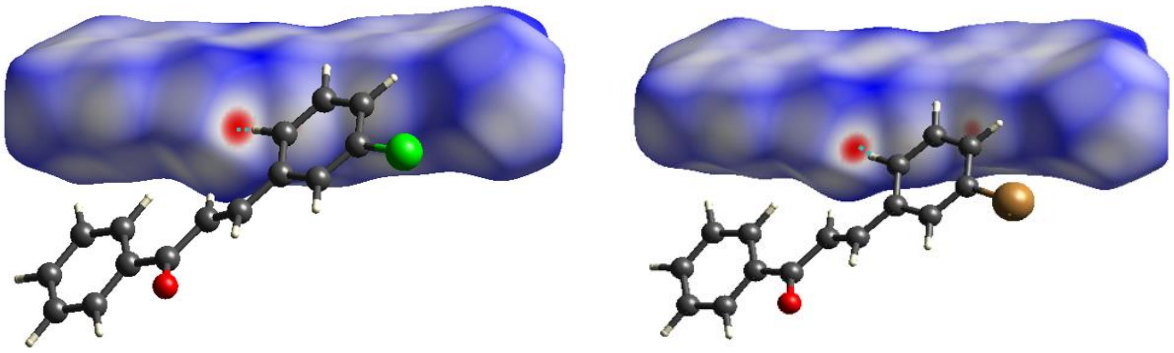

(a) (b)

Interações hidrofóbicas do tipo π ... π e C-H ... π são mostradas no shape index, a região vermelha é uma região aceptora de elétrons enquanto a região azul é uma região doadora de elétrons, na Figura 13 a e b pode-se ver as superfícies para as interações C-H…Cl e C-H...Br respectivamente, as figuras 13 c, d, e e f mostram interações do tipo C-H ... π, a interação C_{15}-H_{15}…Cg2 para o CLC (c) e para o BRC (d), a interação C_{12}-H_{12}…Cg1 para o CLC (e) e para o BRC (f). As interações π...π

podem ser identificadas na superfície por uma região de encontro de dois triângulos, um vermelho e outro azul (Figura 13 g para o CLC e h para o BRC).

Figura 13- Superfície de Hirshfeld Shape Index para as interações (a) C-H...Cl, (b) C-H...Br, (c) C15-H15…Cg2 para o CLC, (d) C15-H15…Cg2 para o BRC, (e) C12-H12…Cg1 para o CLC, (f) C12-H12…Cg1 para o BRC, (g) π...π para o CLC, e (h) π...π para o BRC.

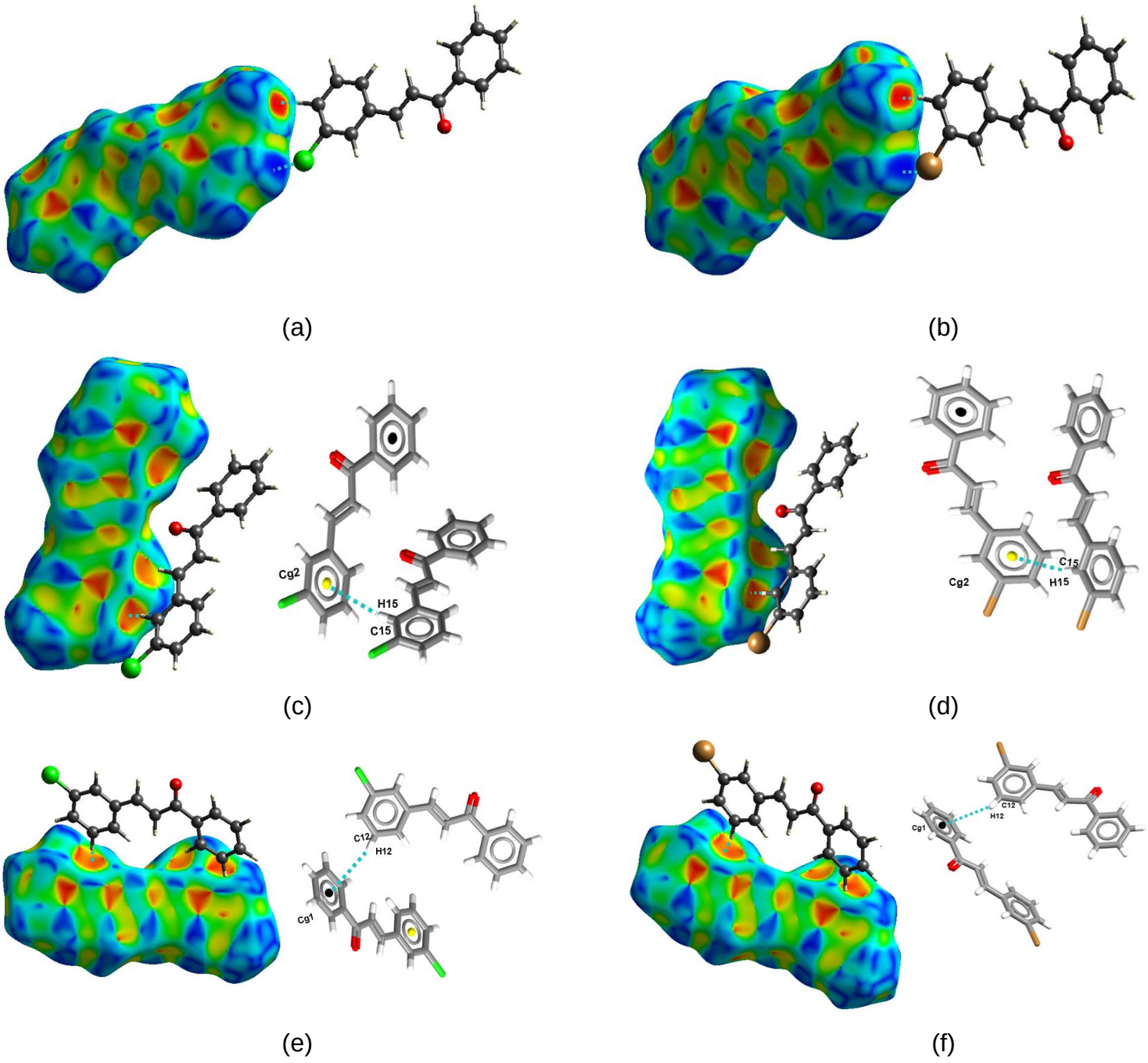

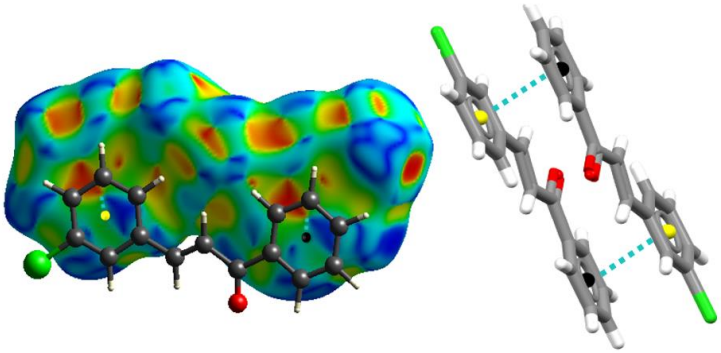

(g)

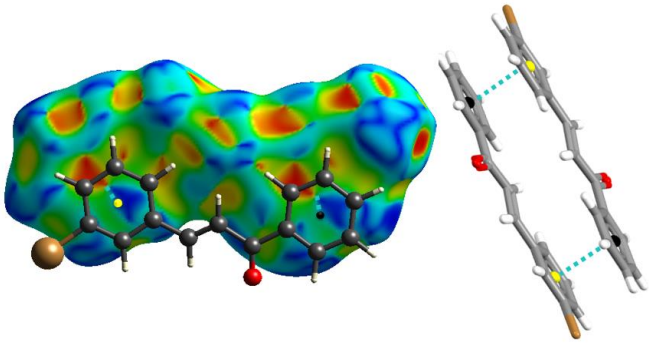

(h)

Os cálculos teóricos mostraram que a troca dos átomos de halogênios não causam grandes mudanças na estrutura molecular. Ademais, foi possível determinar que ambas as estruturas são apropriadas para uso como material óptico não linear. Todos os resultados obtidos estão no artigo “A new isostructural halogenated chalcone with optical properties” publicado no Journal of Molecular Modeling, mostrado a seguir.

4 CONSIDERAÇÕES FINAIS

A cristalografia é uma metodologia que nos permite determinar a composição da estrutura molecular e as posições atômicas na cela unitária, assim como, o arranjo cristalino empregado à difração de raios X e programas computacionais, os dados cristalográficos obtidos podem, nesse contexto, ser utilizados para estudar as propriedades físico-químicas e bioquímicas dessa molécula para encontrar aplicabilidade para esse composto.

Nesse trabalho, realizou-se a elucidação estrutural de um derivado de chalcona inédito, a 3- (3-chlorophenyl) -1-phenylprop-2-en-1-one, foram avaliados os parâmetros estruturais e geométricos e comparados com uma chalcona bromo substituída encontrada na literatura a 3- (3-bromophenyl) -1-phenylprop-2-en-1-one, a partir desta comparação foi possível identificar um caso de isoestruturalidade, em que as estruturas são muito semelhantes.

Desse modo, as interações intermoleculares que contribuem energeticamente para a estabilidade dos cristais foram interações não covalentes “fracas” do tipo π...π, C-H...π e interações de hidrogênio não clássicas C-H...O. Também foram encontradas interações do tipo C-H...Cl ou C-H...Br e C-H...H-C, as duas estruturas cristalizaram no grupo espacial monoclínico $P2_1/c$, os parâmetros de cela unitária são semelhantes e todas as interações identificadas em uma molécula também estão presentes na outra, a sobreposição das moléculas comprova essa similaridade. Todos esses fatores validam a isoestruturalidade dessas chalconas, apesar das diferenças existentes entre os átomos de cloro e bromo (bromo possui 18 elétrons a mais que o cloro além de ser mais eletronegativo). Todos os dados desse estudo juntamente com cálculos de mecânica quântica (realizados pelo Prof. Dr.

Ademir J Camargo) e cálculos de propriedades ópticas não lineares (realizados pelo Prof. Dr. Clodoaldo Valverde) foram publicados em um artigo presente no capitulo 3 (Resultados e Discussões) no Journal of Molecular Modeling.

5 REFERÊNCIAS

ABU, N. et al. The flavokawains : uprising medicinal chalcones. **BioMed Central**, v. 13, 2013.

ALMEIDA, L. R. . et al. Cristalografia: 100 Anos no Caminho da Inovação. Revista Processos Químicos. **Revista Processos Químicos**, v. 16, p. 75–86, 2014.

BLAKE, A. J. . et al. **Crystal Structure Analysis Principles and Practice**. 2ª ed. New York: IUCr – Oxford University Press, 2009.

CHATTERJEE, S. K. **Crystallography and the world of symmetry**. Berlin, Heidelberg: 2008, 2008.

CULLITY, B. D. . **Elements of X-Ray Diffraction**. USA: Addison-Wesley Publishing Company Inc, 2001.

DRENTH, J. **Principles of Proteins X-Ray Crystallography**. New York: Springer Verlag, 1994.

DUARTE, V. S. et al. Benzodioxol Group Driving Supramolecular Arrangement of Two Tri-Methoxy Chalcones onto B -Secretase 1 Enzyme Active Site. **J. Braz. Chem. Soc.**, v. 30, p. 1916–1926, 2019.

GIACOVAZZO, C. . et al. **Fundamentals of Crystallography**. 3ª ed. [s.l.] Oxford University Press, 2011.

GLUSKER, J. P. .; LEWIS, M. .; ROSSI, M. **Crystal Structure Analysis For Chemists and Biologists**. 1ª ed ed. New York: Wiley-VCH, 1994.

GLUSKER, J. P. .; TRUEBLOOD, K. N. . **Crystal Structure Analysis a Primer**. 3ª ed. [s.l.] Oxford University Press, 2010.

GUIDO, R. V. C.; ANDRICOPULO, A. D.; OLIVA, G. Biotecnologia e química medicinal: aplicações em doenças infecciosas. **Estudos Avançados**, v. 24, n. 70, p. 81–98, 2010.

HSIEH, C. et al. Bioorganic & Medicinal Chemistry Letters Synthesis of chalcone derivatives as potential anti-diabetic agents. **Bioorganic & Medicinal Chemistry Letters**, v. 22, n. 12, p. 3912–3915, 2012.

KUSZ, J.; MAŁECKA, M.; CHE, L. Interactions in flavanone and chalcone derivatives : Hirshfeld surface analysis , energy frameworks and global reactivity descriptors. **Acta Crystallographica Section C: Structural Chemistry**, v. 76, p. 212–224, 2020.

MÜLLER, P. . et al. **Crystal Structure Refinement: A Crystallographer's Guide to SHELXL**. New York: Oxford University Press, 2006.

NAPOLITANO, H. B. . et al. Análise da difração de Raios X. **Revista Processos Químicos**, p. 35–45, 2007.

NOWAKOWSKA, Z. A review of anti-infective and anti-inflammatory chalcones. **European Journal of Medicinal Chemistry**, v. 42, p. 125–137, 2007.

OSORIO, M. E. et al. Antimicrobial, Anti-Inflammatory and Antioxidant Activities of Polyoxygenated Chalcones. **J. Braz. Chem. Soc.**, p. 1–19, 2018.

STOUT, G. H. .; JENSEN, L. H. . **X-Ray Structure Determination, A Practical Guide**.

2ª ed. New York: Wiley-Interscience, 1989.

VENCATO, I. Estruturas cristalinas por difração de raios-x. **Cad. Cat. Ens. Fís.**, v. 5, n. 3, p. 168–171, 1988.

VLACK, V. H. L. . **Princípios de Ciência dos Materiais: Reações no estado sólido**. 1ª ed. São Paulo: : Edgard Blucher Ltda., 1970.

WON, S.-J. et al. Synthetic chalcones as potential anti-inflammatory and cancer chemopreventive agents. **European Journal of Medicinal Chemistry**, v. 40, p. 103–112, 2005.

ZAINURI, D. A.; RAZAK, I. A.; ARSHAD, S. Molecular structure , DFT studies and Hirshfeld analysis of anthracenyl chalcone derivatives research communications. **Acta Cryst. E**, v. 74, p. 780–785, 2018.

ANEXO I

SPRINGER NATURE LICENÇA PARA REPRODUÇÃO DO ARTIGO

SPRINGER NATURE LICENSE
TERMS AND CONDITIONS

Mar 29, 2021

This Agreement between Miss. Gabriela Ludovico ("You") and Springer Nature ("Springer Nature") consists of your license details and the terms and conditions provided by Springer Nature and Copyright Clearance Center.

License Number	5038381338382
License date	Mar 29, 2021
Licensed Content Publisher	Springer Nature
Licensed Content Publication	Journal of Molecular Modeling
Licensed Content Title	A new isostructural halogenated chalcone with optical properties
Licensed Content Author	Gabriela S. Ludovico et al
Licensed Content Date	Jan 27, 2021
Type of Use	Thesis/Dissertation
Requestor type	academic/university or research institute
Format	print and electronic
Portion	full article/chapter
Will you be translating?	no
Circulation/distribution	1 - 29
Author of this Springer Nature content	yes

Title	Isostructural Description of Two Halogenated Chalcones
Institution name	Goias State University
Expected presentation date	Mar 2021
Order reference number	1
Requestor Location	Miss. Gabriela Ludovico Rua Paranapuã Qd 24 lt05 parque Iracema Anápolis, Goiás 75063-133 Brazil Attn: Miss. Gabriela Ludovico
Total	0.00 USD

Terms and Conditions

Springer Nature Customer Service Centre GmbH
Terms and Conditions

This agreement sets out the terms and conditions of the licence (the **Licence**) between you and **Springer Nature Customer Service Centre GmbH** (the **Licensor**). By clicking 'accept' and completing the transaction for the material (**Licensed Material**), you also confirm your acceptance of these terms and conditions.

1. Grant of License

1. 1. The Licensor grants you a personal, non-exclusive, non-transferable, world-wide licence to reproduce the Licensed Material for the purpose specified in your order only. Licences are granted for the specific use requested in the order and for no other use, subject to the conditions below.

1. 2. The Licensor warrants that it has, to the best of its knowledge, the rights to license reuse of the Licensed Material. However, you should ensure that the material you are requesting is original to the Licensor and does not carry the copyright of another entity (as credited in the published version).

1. 3. If the credit line on any part of the material you have requested indicates that it was reprinted or adapted with permission from another source, then you should also seek permission from that source to reuse the material.

2. Scope of Licence

2. 1. You may only use the Licensed Content in the manner and to the extent permitted by these Ts&Cs and any applicable laws.

2. 2. A separate licence may be required for any additional use of the Licensed Material, e.g. where a licence has been purchased for print only use, separate permission must be obtained for electronic re-use. Similarly, a licence is only valid in the language selected and does not apply for editions in other languages unless additional translation rights have been granted separately in the licence. Any content owned by third parties are expressly excluded from the licence.

2. 3. Similarly, rights for additional components such as custom editions and derivatives require additional permission and may be subject to an additional fee. Please apply to Journalpermissions@springernature.com/bookpermissions@springernature.com for these rights.

2. 4. Where permission has been granted **free of charge** for material in print, permission may also be granted for any electronic version of that work, provided that the material is incidental to your work as a whole and that the electronic version is essentially equivalent to, or substitutes for, the print version.

2. 5. An alternative scope of licence may apply to signatories of the STM Permissions Guidelines, as amended from time to time.

3. Duration of Licence

3. 1. A licence for is valid from the date of purchase ('Licence Date') at the end of the relevant period in the below table:

Scope of Licence	Duration of Licence
Post on a website	12 months
Presentations	12 months
Books and journals	Lifetime of the edition in the language purchased

4. Acknowledgement

4. 1. The Licensor's permission must be acknowledged next to the Licenced Material in print. In electronic form, this acknowledgement must be visible at the same time as the figures/tables/illustrations or abstract, and must be hyperlinked to the journal/book's homepage. Our required acknowledgement format is in the Appendix below.

5. Restrictions on use

5. 1. Use of the Licensed Material may be permitted for incidental promotional use and minor editing privileges e.g. minor adaptations of single figures, changes of format, colour and/or style where the adaptation is credited as set out in Appendix 1 below. Any other changes including but not limited to, cropping, adapting, omitting material that affect the meaning, intention or moral rights of the author are strictly prohibited.

5. 2. You must not use any Licensed Material as part of any design or trademark.

5. 3. Licensed Material may be used in Open Access Publications (OAP) before publication by Springer Nature, but any Licensed Material must be removed from OAP sites prior to final publication.

6. Ownership of Rights

6. 1. Licensed Material remains the property of either Licensor or the relevant third party and any rights not explicitly granted herein are expressly reserved.

7. Warranty

IN NO EVENT SHALL LICENSOR BE LIABLE TO YOU OR ANY OTHER PARTY OR ANY OTHER PERSON OR FOR ANY SPECIAL, CONSEQUENTIAL, INCIDENTAL OR INDIRECT DAMAGES, HOWEVER CAUSED, ARISING OUT OF OR IN CONNECTION WITH THE DOWNLOADING, VIEWING OR USE OF THE MATERIALS REGARDLESS OF THE FORM OF ACTION, WHETHER FOR BREACH OF CONTRACT, BREACH OF WARRANTY, TORT, NEGLIGENCE, INFRINGEMENT OR OTHERWISE (INCLUDING, WITHOUT LIMITATION, DAMAGES BASED ON LOSS OF PROFITS, DATA, FILES, USE, BUSINESS OPPORTUNITY OR CLAIMS OF THIRD PARTIES), AND
WHETHER OR NOT THE PARTY HAS BEEN ADVISED OF THE POSSIBILITY OF SUCH DAMAGES. THIS LIMITATION SHALL APPLY NOTWITHSTANDING ANY FAILURE OF ESSENTIAL PURPOSE OF ANY LIMITED REMEDY PROVIDED HEREIN.

8. Limitations

8. 1. ***BOOKS ONLY:*** Where **'reuse in a dissertation/thesis'** has been selected the following terms apply: Print rights of the final author's accepted manuscript (for clarity, NOT the published version) for up to 100 copies, electronic rights for use only on a personal website or institutional repository as defined by the Sherpa guideline (www.sherpa.ac.uk/romeo/).

8. 2. For content reuse requests that qualify for permission under the STM Permissions Guidelines, which may be updated from time to time, the STM Permissions Guidelines supersede the terms and conditions contained in this licence.

9. Termination and Cancellation

9. 1. Licences will expire after the period shown in Clause 3 (above).

9. 2. Licensee reserves the right to terminate the Licence in the event that payment is not received in full or if there has been a breach of this agreement by you.

Appendix 1 — Acknowledgements:

For Journal Content:
Reprinted by permission from [**the Licensor**]: [**Journal Publisher** (e.g. Nature/Springer/Palgrave)] [**JOURNAL NAME**] [**REFERENCE CITATION** (Article name, Author(s) Name), [**COPYRIGHT**] (year of publication)

For **Advance Online Publication papers:**
Reprinted by permission from [**the Licensor**]: [**Journal Publisher** (e.g.

Nature/Springer/Palgrave)] [**JOURNAL NAME**] [**REFERENCE CITATION** (Article name, Author(s) Name), [**COPYRIGHT**] (year of publication), advance online publication, day month year (doi: 10.1038/sj.[JOURNAL ACRONYM].)

For Adaptations/Translations:
Adapted/Translated by permission from [**the Licensor**]: [**Journal Publisher** (e.g. Nature/Springer/Palgrave)] [**JOURNAL NAME**] [**REFERENCE CITATION** (Article name, Author(s) Name), [**COPYRIGHT**] (year of publication)

Note: For any republication from the British Journal of Cancer, the following credit line style applies:

Reprinted/adapted/translated by permission from [**the Licensor**]: on behalf of Cancer Research UK: : [**Journal Publisher** (e.g. Nature/Springer/Palgrave)] [**JOURNAL NAME**] [**REFERENCE CITATION** (Article name, Author(s) Name), [**COPYRIGHT**] (year of publication)

For **Advance Online Publication** papers:
Reprinted by permission from The [**the Licensor**]: on behalf of Cancer Research UK: [**Journal Publisher** (e.g. Nature/Springer/Palgrave)] [**JOURNAL NAME**] [**REFERENCE CITATION** (Article name, Author(s) Name), [**COPYRIGHT**] (year of publication), advance online publication, day month year (doi: 10.1038/sj.[JOURNAL ACRONYM])

For Book content:
Reprinted/adapted by permission from [**the Licensor**]: [**Book Publisher** (e.g. Palgrave Macmillan, Springer etc) [**Book Title**] by [**Book author**(s)] [**COPYRIGHT**] (year of publication)

Other Conditions:

Version 1.3

Questions? customercare@copyright.com or +1-855-239-3415 (toll free in the US) or +1-978-646-2777.

ANEXO II

Artigo: A new isostructural halogenated chalcone with optical properties

Journal of Molecular Modeling (2021) 27: 52
https://doi.org/10.1007/s00894-021-04673-9

ORIGINAL PAPER

A new isostructural halogenated chalcone with optical properties

Gabriela S. Ludovico[1] · Itallo H. S. Barros[1] · Loide O. Sallum[1] · Rosa S. Lima[2] · Clodoaldo Valverde[1,3] · Ademir J. Camargo[1] · Basílio Baseia[4,5] · Hamilton B. Napolitano[1]

Received: 10 September 2020 / Accepted: 13 January 2021 / Published online: 27 January 2021

Abstract

Chalcones are organic compounds that present a number of properties. This study presents a comprehensive structural description of a new derivative of a chlorine-substituted chalcone in comparison with a bromine chalcone. Also, supermolecule and sum-over-state approach were used to describe the optical properties of these structures regarding the substitution of the bromine by the chlorine atom. In addition, the electrical properties, dipole moment, linear polarizability, and second IDRI hyperpolarizability were calculated. The linear refractive index and the third-order nonlinear macroscopic susceptibility were evaluated as a function of the applied electric field frequency. Furthermore, the quantum mechanics calculations that were implemented at the M06-2X/6-311++G(d,p) level of the theory for these isostructural chalcones indicate that the change in halogen atoms does not cause meaningful changes in their conformation. Finally, we can postulate that side-to-side and the antiparallel interactions are the interaction forces that drive the crystal growth for new isostructural chalcones. The NLO properties showed title compounds that are good candidates for use as NLO materials.

Keywords Isostructural chalcones · X-ray diffraction · NLO properties · Sum-over-state

Introduction

Chalcones are a group of organic compounds derived from natural products, which can be obtained synthetically. They consist of two aromatic rings linked by an α, β unsaturated carbonyl system [1–3]. Chalcones have many biological activities, such as anticancer, anti-inflammatory, antioxidant, antifungal, and antidiabetic activities [4–9]. There is a close relationship between their activities and the substituents present on their aromatic rings. Additionally, halogen substituents can promote changes in biological activities without causing structural changes [10, 11]. Given the recent development of photonics and discoveries in molecular modeling, there has been a growing interest in materials exhibiting nonlinear optical (NLO) properties.

In this context, organic molecules have been the focus of a great deal of research because of the ease in manipulating their structures and as a result obtaining structures offering important NLO properties [12, 13]. Thus, organic crystals have attracted great interest for their application in photonics [14, 15] as well as spectroscopy [16, 17], frequency modulators [18], and data transmission [19]. Organic crystals generally have high nonlinear characteristics and a versatile synthetic route, thus allowing us the production of materials with high nonlinearity. The chalcone derivatives, being organic compounds, are easy to handle, allowing the improvement of NLO properties. Compounds with similar or even the same crystalline packing are known as isostructures, and the relationship between the similarity and the NLO properties is important in developing new isostructural materials [20]. Also, studies show that halogen atoms like chlorine and bromine are very suitable substitutes for isostructures [3, 20].

Due to the importance of the substituents in the physicochemical and biological properties of organic molecules and

This paper belongs to Topical Collection XX - Brazilian Symposium of Theoretical Chemistry (SBQT2019).

✉ Hamilton B. Napolitano
hbnapolitano@gmail.com

[1] Grupo de Química Teórica e Estrutural de Anápolis, Universidade Estadual de Goiás, Anápolis, GO 75001-970, Brazil

[2] Faculdade do Instituto Brasil de Ciência e Tecnologia, Anápolis, GO 75133-050, Brazil

[3] Laboratório de Modelagem Molecular Aplicada e Simulação, Universidade Paulista, Goiânia, GO 74845-090, Brazil

[4] Instituto de Física, Universidade Federal de Goiás, Goiânia, GO 74690-900, Brazil

[5] Departamento de Física, Universidade Federal da Paraíba, João Pessoa, PB 58051-970, Brazil

to better understand the influence of halogens as substituents in chalcones, this paper conducts the study of a new chalcone derivative, 3-(3-chlorophenyl) -1-phenylprop-2-en-1-one (CLC) compared to 3-(3-bromophenyl) -1-phenylprop-2-en-1-one (BRC) [21], by structural elucidation, supramolecular arrangement, and optical properties. Molecular structure was characterized by monocrystalline X-ray diffraction and supramolecular arrangement by Hirshfeld Surface. The DFT/CAM-B3LYP/6-311++G(d,p) supermolecule (SM) approach and sum-over-state method were used to analyze NLO properties in a crystalline equivalent environment.

Experimental and computational procedures

Synthesis and crystallization

The chalcone CLC was synthesized using a volumetric flask reactor of 50 mL size, to which was added 10 mL of methanol, acetophenone (2.5 mM), and 3-chlorobenzaldehyde (2.5 mM) with a high purity rate. Then, five drops of 20% aqueous potassium hydroxide solution were added into the reaction medium. The reaction mixture was shaken for 30 minutes at room temperature. At the end of the reaction time, the mixture was treated with HCl solution (10%) and washed with water, and then, dichloromethane was added to the separation funnel to drag out the organic phase (the average yield was 75%). Dichloromethane was evaporated at room temperature for 24 h, and then, isopropyl alcohol was added for compound recrystallization, as shown in Scheme 1. The synthesis process was accompanied by thin-layer chromatography. The Claisen-Schmidt methodology was used in the experimental protocol. Infrared spectra (IR) were recorded on a PerkinElmer Frontier in the range of 4000–400 cm^{-1} using the attenuated total reflection (ATR) technique (Fig. 1). Nuclear magnetic resonance (NMR) spectra were recorded on a Bruker Avance III, operating at 500.13 MHz for ^{1}H and 125.77 MHz for ^{13}C, equipped with a 5 mm TBI probe (^{1}H, ^{13}C and XBB). The frequency of radio frequency radiation absorbed by a given nucleus is strongly affected by its chemical environment [22] (electrons and near nucleus). The spectrum shows increased chemical displacement expressed in parts per million (ppm) of the right to left [23].

Yellow solid, 75% yield. IR νmax: 3538 (C-sp^2), 3066 (C=C, sp^2, alkene), 1664 (C=O, ketone), 1605 (C=C, aromatic ring), 1446, 1421,1304, 1221, 1079, 1021, 970, 904, 861 (Ar-C, off plan), 770 (C-Cl), 702. ^{1}H NMR [500 MHz, δ (ppm), DMSO-d6]: 8.09 (ddd, J = 1,7; 1,6; 0,5, H-15), 7,80 (d, J = 15,7 Hz, H-9), 7.68 (m, H-2 e H-4), 7,42 (t, J = 7.8 Hz, H-12), 7.52 (ddd, H-13), 7.60 (m,H-1, H-5), 7.44 (tt, H-3), 7,39 (ddd, H-11), 7,26 (d, J = 16,0, H-8). ^{13}C NMR [125,77 MHz, DMSO-d6]190.1 (C-7), 143.1 (C-9), 137.9 (C-6), 136,7 (C-14), 135.0 (C-10), 133.3 (C-12), 133.0 (C-13), 123.3(C-8), 128,7 (C-1, C-5), 130.2 (C-2, C-4), 130.4 (C-3), 128,6 (C-15), 126,8 (C-11).

Crystallographic characterization

A CLC single crystal was chosen for the X-ray diffraction experiment, which was undertaken on a Bruker APEX-II CCD diffractometer with MoKα radiation at a temperature of 296 K. The structure was solved by direct methods using the SHELXS [24] program and substituents using the SHELXL [25] program on the OLEX2 platform [26]. Packing and interactions were analyzed using the Mercury program [27], and the structure data was deposited in the Cambridge Crystallography Data Center (CCDC) with code 2019801. The crystallographic data of BRC is available on code 601146. The Hirshfeld surface (HS) is an important tool to understand the contacts between atoms, the packing of the molecules in the crystal, and the nature of the interactions [28]. Using the Crystal Explorer software, HS and fingerprint analysis of CLC and BRC molecules were performed. The d_{norm}, d_e, and d_i allow us to analyze the strong N–H...O, O–H....O, and O–H....N and weak C–H....O hydrogen interactions, whereas the shape index shows the hydrophobic interactions involving conjugated π systems C–H...π and π...π [29]. Also, the HS calculates a weight function w_a (r) for each atom of the molecule [30]; Equation 1 shows this function.

$$w_a(r) = p_a^{at}(r) / \sum_{i\epsilon \text{ molecule}} p_i^{at}(r) \quad (1)$$

where $p_i^{at}(r)$ are electron densities of atoms. These atomic densities are used to calculate the density of the molecule in the crystal through a weight function (W),

$$W(r) = \frac{\sum_{i\epsilon \text{ molecule}} \rho_i^{at}(r)}{\sum_{i\epsilon \text{ crystal}} \rho_i^{at}(r)}, \quad (2)$$

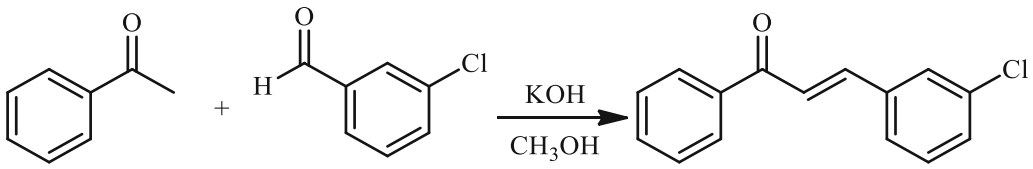

Scheme 1 Chemical scheme of the synthesis of chalcone CLC

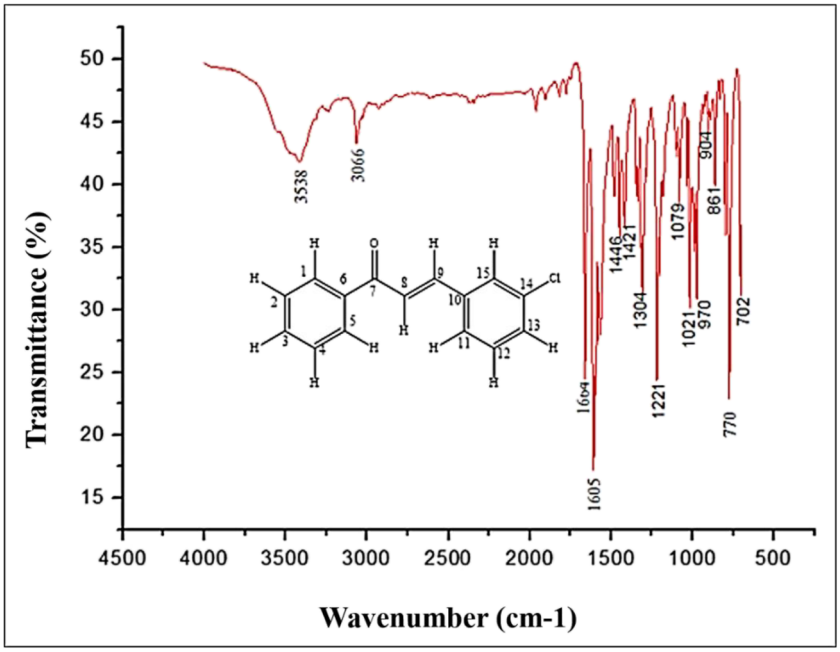

Fig. 1 Infrared graphic to characterize the CLC

which simply means the ratio of the sum of the atom's density of the molecule to the sum of the atom's densities of the crystal [31].

Theoretical and computational procedures

The quantum mechanics calculations were carried out at the M06-2X/6-311++G(d,p) level of the theory using Gaussian16 [32] program package for BRC and CLC compounds. The M06-2X is a hybrid meta-exchange correlation functional, and with the basis set 6-311++G(d,p), good geometric structures were taken [33]. Twice the nonlocal exchange (2X) is applied in the noncovalent interactions and parametrized for long-range interactions [34]. The input used in the calculations (atom coordinates) was taken from the X-ray data. For each compound, only the hydrogen atom geometric parameters were optimized. The basis set superposition errors (BSSE) for the interaction energies were corrected using the counterpoise [35, 36] procedure implemented in the g16 program. The quantum theory of atoms in molecules (QTAIM) [37] was analyzed by the Multiwfn program (version 3.7) [38], and it is a powerful tool to better understand the nature of the dimer interaction energies.

Nonlinear optical properties

The SM method was used to simulate the polarization effect of the crystalline environment around the asymmetric unit [39]. For this purpose, a bulk was created (see scheme in Fig. 2) for the two compounds, both with 13,500 molecules and each molecule with 28 atoms totalizing 378,000 atoms.

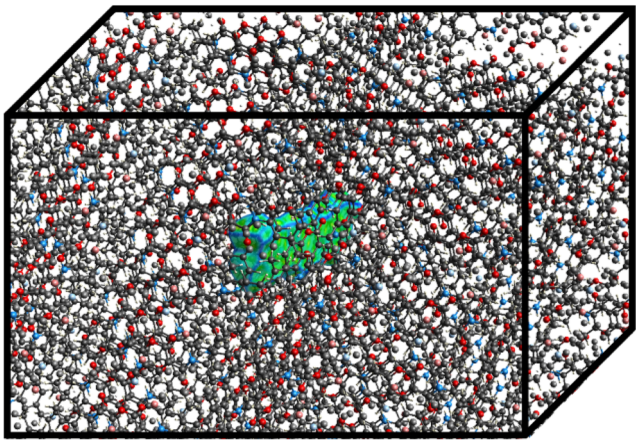

Fig. 2 Bulk scheme for the synthesis of chalcone CLC

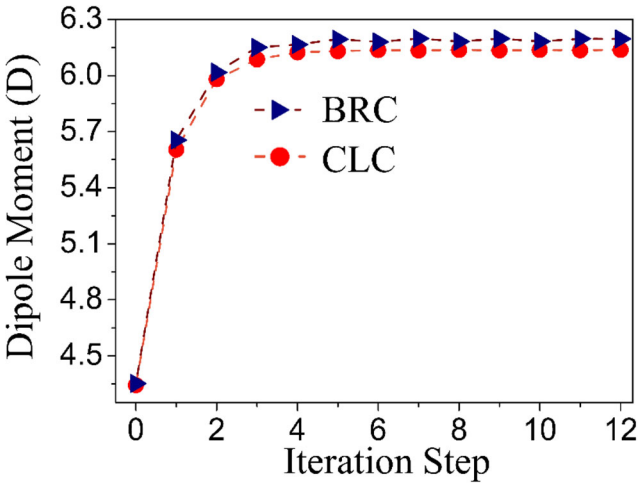

Fig. 3 Graph of dipole moment evolution with the iteration numbers

Table 1 Crystallographic and refinement data for CLC and BRC

Crystal data	CLC	BRC
Chemical formula	$C_{15}H_{11}ClO$	$C_{15}H_{11}BrO$
M_r	242.69	287.15
Crystal system, space group	$P2_1/_C$	$P2_1/_C$
Temperature (K)	296	100
a, b, c (Å)	14.100(3), 7.4948(16), 11.230(3)	14.3238(2), 7.4913(1), 11.2786(2)
α, β, γ (°)	90, 101.009(4), 90	90, 100.325(1), 90
V (Å^3)	1164.9(5)	1190.64(3)
Z	4	4
μ (mm^{-1})	0.306	3.43
$R[F^2 > 2\sigma(F^2)]$	0.0428	0.030
S	1.026	1.10
No. of reflections	2852	7339
No. of parameters	154	154

The SM approach consists of considering the atoms around the colored molecule, in the present case green, as punctual charges, and thus, the dominant intermolecular interactions present are calculated. The SM method is an iterative DFT computed process with functional CAM-B3LYP/6-311++ G(d,p) which ends with the convergence of the total dipole [40–42]; see Fig. 3.

The iterative process of the SM approach is carried out in several steps: initially we determine the electrical charge of each atom of the asymmetric unit using the Chelpg method, which is made by adjusting the molecular electrostatic potential. The partial atomic electric charges of each atom of the asymmetric unit are then placed on each atom of the bulk. This iterative procedure is done until the convergence of the total dipole moment is reached. The theoretical method of SM presented results close to those of experiments according to references [39, 43, 44]. In this way, for the total dipole moment, we have,

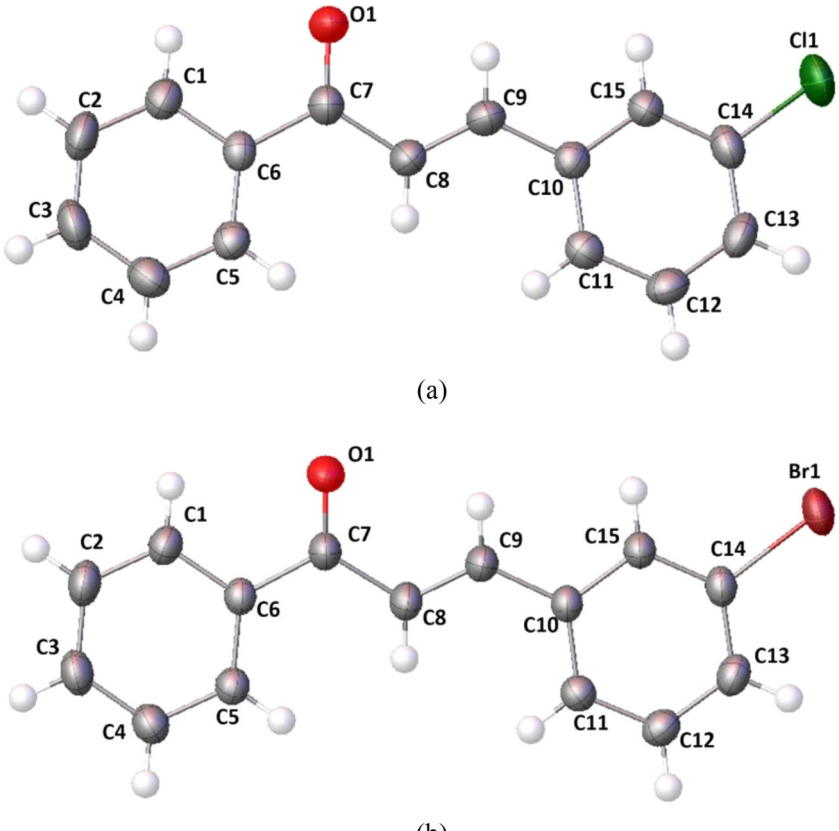

Fig. 4 The ORTEP representation with 75% probability of **a** CLC and **b** BRC

Table 2 Hydrogen-bond geometry (Å, °) for CLC and BRC

	D – H···A	D – H	H···A	D···A	D – H···A	Symmetry code
CLC	C11–H11···O1	0.93	2.49	3.399	165	x,1/2-y,1/2 + z
	C13–H13···Cl1	0.93	2.99	3.905	167	-x,-y,1-z
	C5–H5···O1	0.93	2.49	3.399	164	x,1/2-y,1/2 + z
	C8–H8···O1	0.93	2.78	3.684	166	x,1/2-y,1/2 + z
	C2–H2···H3–C3	0.93	2.51	4.111	146	2-x,1-y,1-z
	C3–H3···H2–C2	0.93	2.51	4.111	154	2-x,1-y,1-z
BRC	C11–H11···O1	0.93	2.50	3.411	166	x,1/2-y,1/2 + z
	C13–H13···Br1	0.93	3.09	4.000	164	-x,-y,1-z
	C5–H5···O1	0.93	2.79	3.717	172	x,1/2-y,1/2 + z
	C8–H8···O1	0.93	2.79	3.700	165	x,1/2-y,1/2 + z
	C2–H2···H3–C3	0.93	2.62	4.221	143	2-x,1-y,1-z
	C3–H3···H2–C2	0.93	2.62	4.221	155	2-x,1-y,1-z

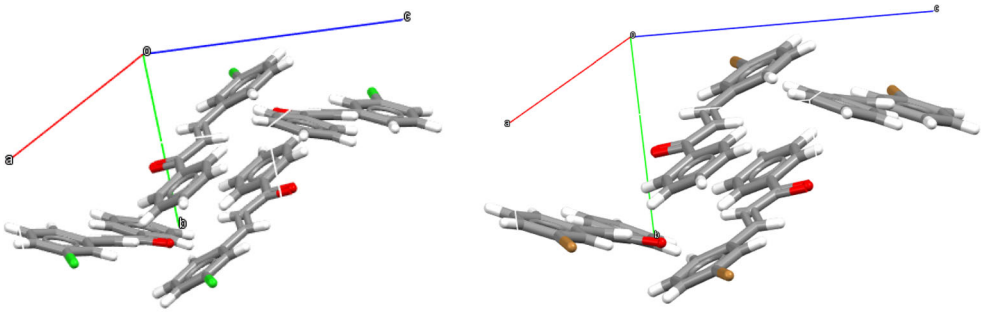

Fig. 5 Crystal packaging **a** for the molecule of CLC, **b** for the molecule of BRC. The crystallographic arrangement grows in direction c, sustained by C–H...O and π…π interactions, showing that just like intermolecular interactions the topography follows the same pattern

(a) (b)

$$\mu = \left(\mu_x^2 + \mu_y^2 + \mu_z^2\right)^{\frac{1}{2}}, \quad (3)$$

where the values of the average linear polarizability can be defined as,

$$\langle\alpha\rangle = \frac{\alpha_{xx} + \alpha_{yy} + \alpha_{zz}}{3} \quad (4)$$

whereas the average linear polarizability $\langle\alpha\rangle$ can be related to the linear refractive index (n_0) of the crystal by the Clausius-Mossotti formula [45],

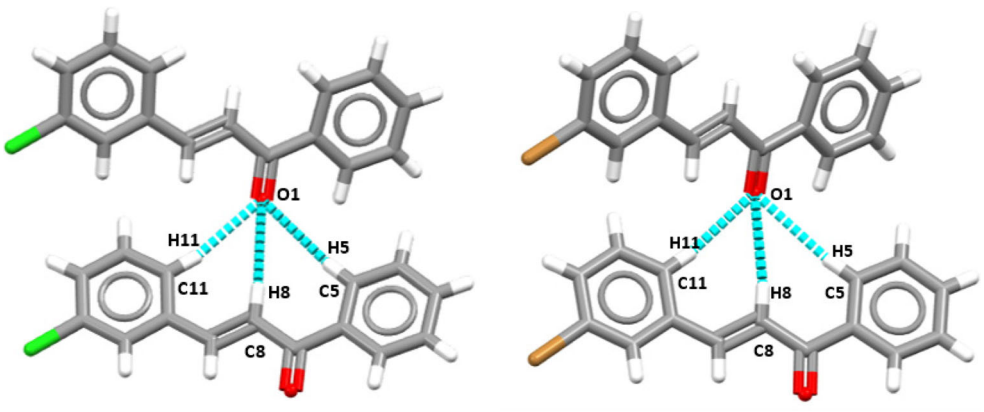

Fig. 6 Molecular arrangement to show interactions **a** CLC C11–H11…O1, C5–H5…O1, C8–H8…O1 and **b** BRC C11–H11…O1, C5–H5…O1, C8–H8…O1; these interactions grow in the c direction

(a) (b)

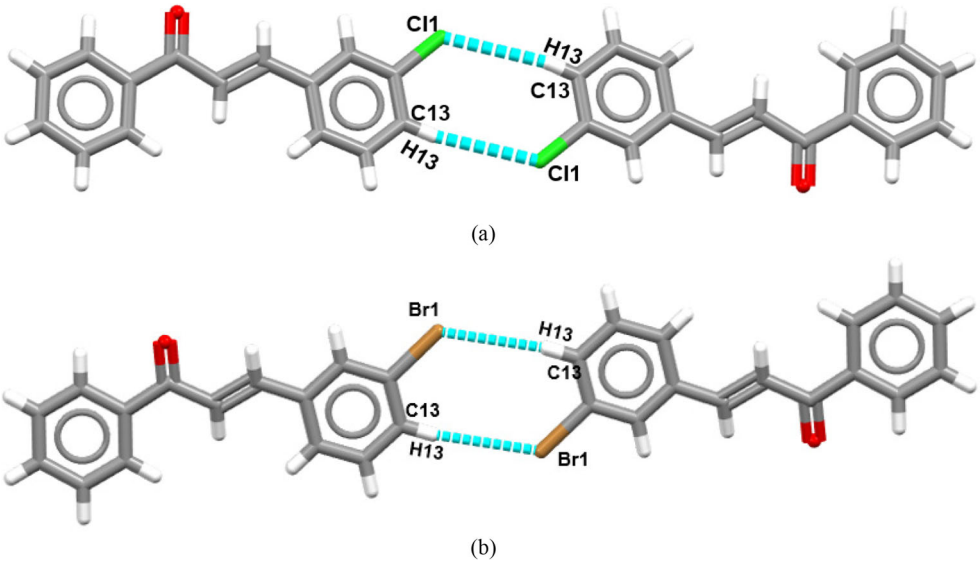

Fig. 7 Molecular arrangement to show interactions **a** CLC C13–H13…Cl1 and **b** BRC C13–H13…Br1; these interactions grow in direction a

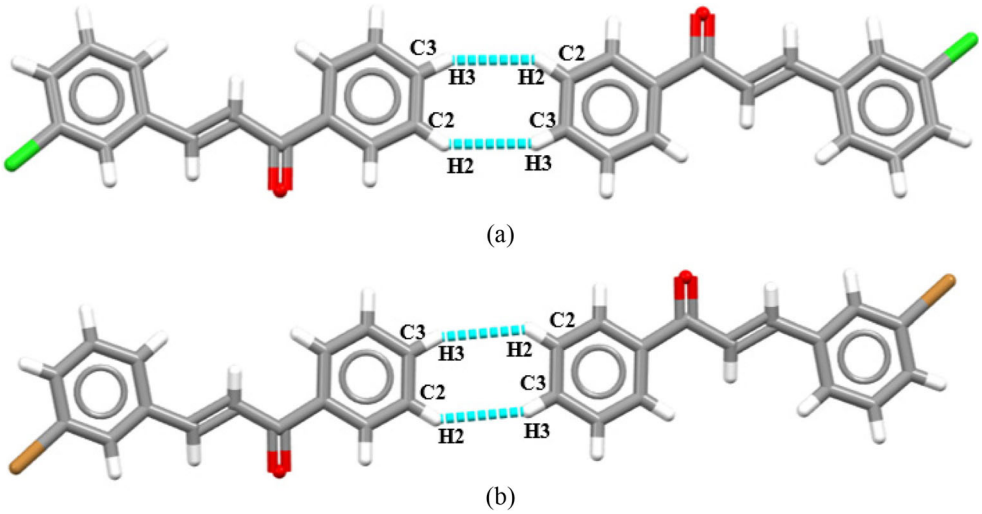

Fig. 8 Molecular arrangement to show interactions **a** CLC C2–H2 ... C3–H3, C3–H3… C2–H2 and **b** BRC C2–H2... C3–H3, C3–H3… C2–H2; these interactions grow in direction a

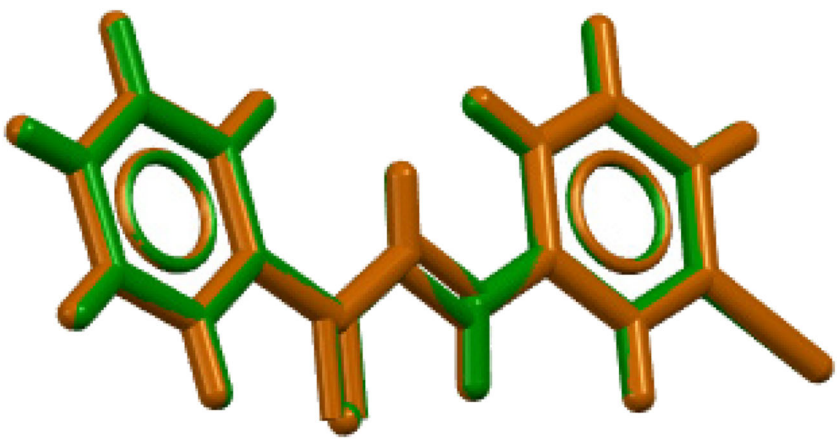

Fig. 9 Overlap of CLC and BRC structures relative to the aromatic ring of chalcone, where CLC is represented in green and BRC in brown

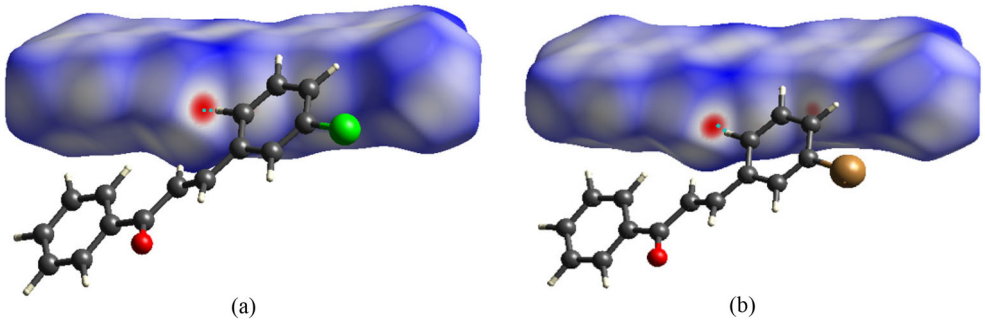

Fig. 10 The d_{norm} for **a** CLC; **b** BRC, where the blue area represents the absence of interactions, and the red dots are areas with interactions, that is, the region where electrons are exchanged

$$\frac{{n_0}^2-1}{{n_0}^2+2}=\frac{4\pi N}{3}\langle\alpha\rangle, \tag{5}$$

where N is the number of molecules per unit volume of the unit cell. Here we will not study the first molecular hyperpolarizability due to crystal symmetry, because the second-order nonlinear macroscopic susceptibility is null. The value of the second hyperpolarizability [46] is obtained in the form,

$$\langle\gamma\rangle=\frac{1}{15}\sum_{i,j=x,y,z}\left(\gamma_{iijj}+\gamma_{ijij}+\gamma_{ijji}\right). \tag{6}$$

The second static average hyperpolarizability can be simplified using the symmetry relation $\gamma_{xxyy} = \gamma_{yyxx} = \gamma_{xyyx} = \gamma_{yxxy}$as proposed by Kleinman [47],

$$\langle\gamma(0;0,0,0)\rangle=\frac{1}{5}\left[\gamma_{xxxx}+\gamma_{yyyy}+\gamma_{zzzz}+2\left(\gamma_{xxyy}+\gamma_{xxzz}+\gamma_{yyzz}\right)\right]. \tag{7}$$

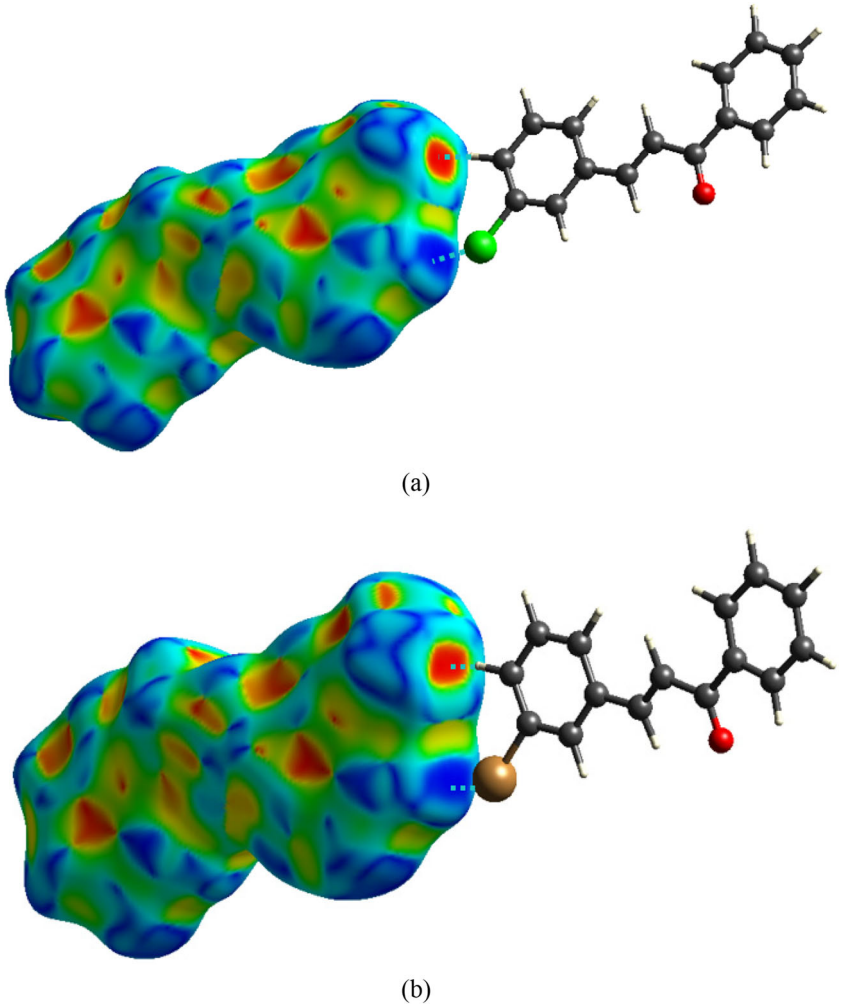

Fig. 11 HS shape index for **a** C–H…Cl interaction (compound CLC) and **b** C–H…Br interaction (compound BRC); in shape index, the red region is an electron acceptor region while the blue region is an electron donor region

The average second hyperpolarizability $\langle\gamma(-\omega;\omega,\omega,-\omega)\rangle$ is related to the intensity-dependent refractive index (IDRI) for small frequencies [48], given by

$$\langle\gamma(-\omega;\omega,\omega,-\omega)\rangle \cong 2\langle\gamma(-\omega;\omega,0,0)\rangle - \langle\gamma(0;0,0,0)\rangle. \quad (8)$$

The sum-over-state (SOS) approach will be used to calculate the second hyperpolarizability. The SOS approach has been widely used to calculate the second molecular hyperpolarizability in organic compounds [49–59]. The benefit of the SOS approach is that it truncates the sum of states, as the significant contribution occurs in only a few excited states. Furthermore, the excitation energies linked to the dipole moment transitions between the ground state and excited states wave functions depend on the precision of the theoretical method used in the SOS approach. The equations used in the SOS approach for calculating the second hyperpolarizability are defined as,

$$\gamma_{xyzw}(-\omega_s;\omega_1,\omega_2,\omega_3) = \widehat{P}[x(-\omega_s),y(\omega_1),z(\omega_2),w(\omega_3)](\Omega_1-\Omega_2), \quad (9)$$

where

$$\Omega_1 = \sum_{i\neq 0}\sum_{j\neq 0}\sum_{k\neq 0}\left[\frac{\mu^x_{0i}\overline{\mu^y_{ij}}\,\overline{\mu^z_{jk}}\mu^w_{k0}}{(\varepsilon_i-\omega_s)(\varepsilon_j-\omega_2-\omega_3)(\varepsilon_k-\omega_3)}\right], \Omega_2 = \sum_{i\neq 0}\sum_{j\neq 0}\left[\frac{\mu^x_{0i}\mu^y_{i0}\mu^z_{0j}\mu^w_{j0}}{(\varepsilon_i-\omega_s)(\varepsilon_i-\omega_2)(\varepsilon_j-\omega_3)}\right],$$

where $\omega_s = \sum_i \omega_i$, and ω is frequency of external fields, $\mu^x_{ij} = \langle i|\widehat{\mu}^x|j\rangle$, $\overline{\mu^x_{ij}} = \mu^x_{ij}-\mu^x_{00}\delta_{ij}$, x, y, z denote the directions; ε_i is the excitation energy of the excited state i in relation to the ground state. $\widehat{P}$ is permutation operator, for γ. μ^x_{ij} is x component of transition dipole moment between state i and j.

Third-order nonlinear susceptibility χ^3 [45–47, 60] is related to the second hyperpolarizability as follows

$$\chi^{(3)}(-\omega;\omega,\omega,-\omega) = f^4\frac{N\langle\gamma(-\omega;\omega,\omega,-\omega)\rangle}{\epsilon_o V}, \quad (10)$$

where N is the number of molecules per unit volume of the unit cell, while f is the Lorentz field correction factor, defined as

$$f = \frac{({n_0}^2+2)}{3}. \quad (11)$$

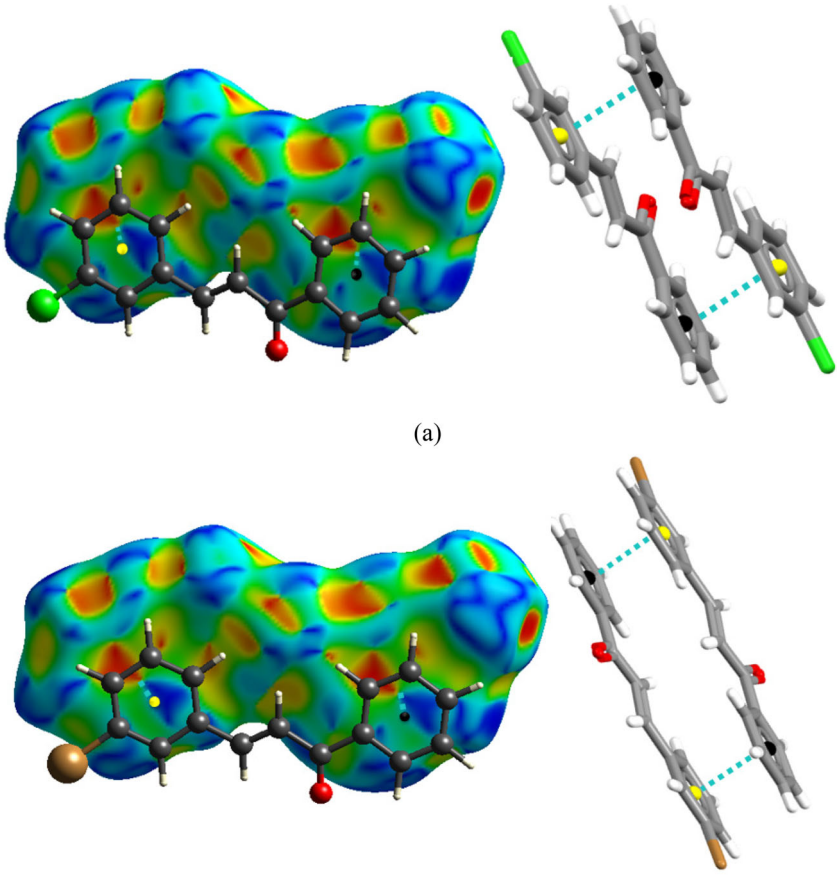

(a)

(b)

Fig. 12 HS shape index for π...π interactions **a** CLC; **b** BRC

All computational calculations related to the linear and nonlinear electrical parameters of the compounds were performed using the Gaussian-09 [61] software package.

Results and discussion

Isostructural solid-state

Both molecules crystallized in the $P2_1/c$ monoclinic space group with unit cell parameters a = 14,100 (3) Å, b = 7,4948 (16) Å, c = 11,230 (3) Å, and β = 101,009 (4) for CLC and a = 14,3238 (2) Å, b = 7,4913 (1) Å, c = 11.2786 (2) Å, and β = 100.325 (1) for BRC. Crystallographic and refinement data are shown in Table 1 and the molecular structure in Fig. 4. These molecules are composed of two aromatic rings linked by an unsaturated carbonyl chain with a chlorine substituent at the meta position attached to one ring of the CLC molecule (Fig. 4a) and a bromine substituent at the same position on the BRC molecule (Fig. 4b), which make compression a way to achieve insights on supra molecular topography and NLO properties.

Both crystalline arrangements (Fig. 5) are maintained by the interactions C–H...O (Figs. 6a and b), dimers of C–H...Cl (Fig. 7a) or C–H...Br (Fig. 7b), besides contacts of type C–H…π and π…π. C–H...H–C interactions are also present (Fig. 8). For both solid-state systems, the intermolecular interactions and topography follow the same pattern [2, 21, 62]. Table 2 shows the non-classical interactions of CLC and BRC crystals, as well as the distances of the bonds.

All interactions observed in CLC are also present in BRC, with slight differences in donor-acceptor distance, such as for CH...O, where the distance H...A of C11-H11...O1 (CLC) is 2.49 Å similar to the BRC distance from C11–H11...O1 (2.50 Å). This example shows no change in the parameters of interactions when chlorine replaces bromine. The packing (Fig. 5) follows the same pattern, since the observed interactions are similar. The overlay (Fig. 9) shows the replacement of bromine substituent with chlorine does not change the molecular structure.

The d_{norm} is shown in Fig. 10, and the red dot on the surface represents a H...O interaction, as in Fig. 10a which shows the interaction C11–H11...O1 of CLC and in Fig. 10b which shows the interaction C11–H11... O1 for BRC. The HS shape index is used to identify C–H...π, π...π, and other hydrophobic interactions. In Fig. 11, H…CL and H…Br interactions are represented; the red concave region represents an electron acceptor region and the blue convex region is an electron donor area. The C13–H13…Cl1 and C13–H13…Br1 interactions form dimers that provide more stability for the CLC and BRC compounds.

The π...π interactions for the CLC and BRC molecules are a dimer that also contributes to packaging stability and are shown in Fig. 12a (Cg1…Cg2 and Cg2…Cg1) and 12b (Cg1…Cg2 and Cg2…Cg1); these interactions can be identified in the HS shape index by a meeting region of two triangles, one red and the other blue. Figure 13a, b, c, and d show C–H...π interactions that in HS shape index can be seen in a red concave region. Figure 13a shows the C12–H12…Cg1

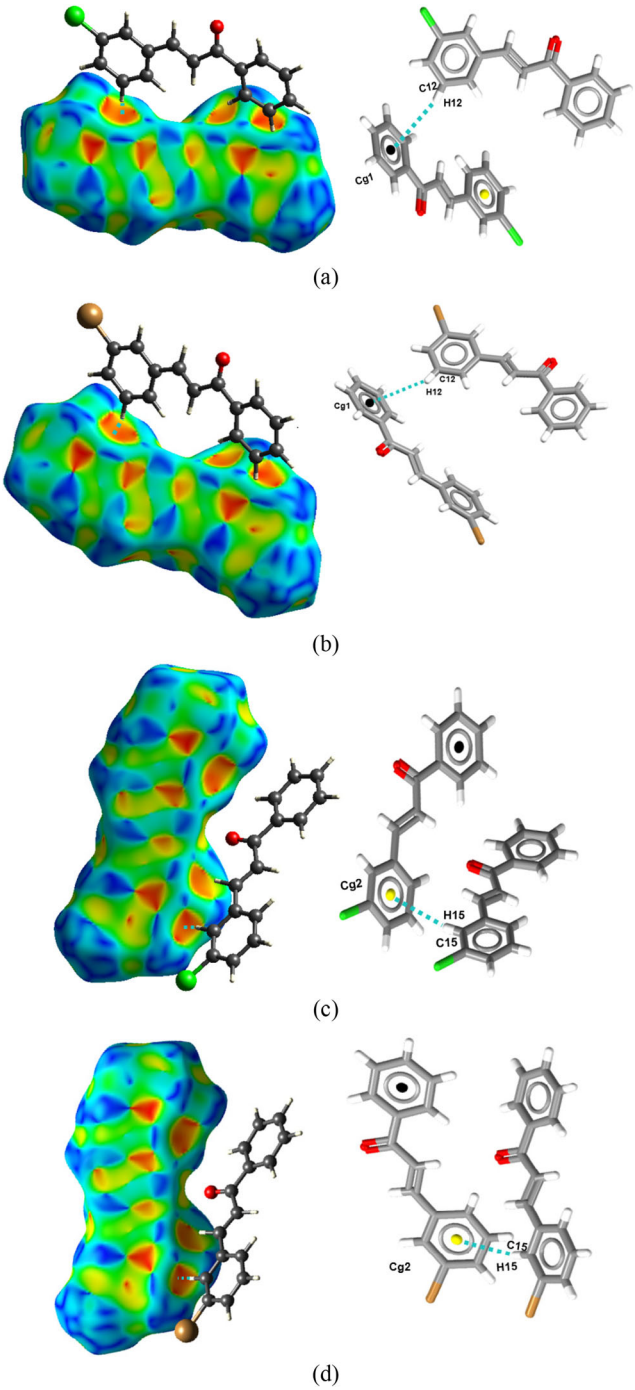

Fig. 13 HS shape index for C–H…π interactions **a** C–H…Cg1 for CLC; **b** C–H…Cg1 for BRC; **e** C–H…Cg2 for CLC and **f** C–H…Cg2 for BRC

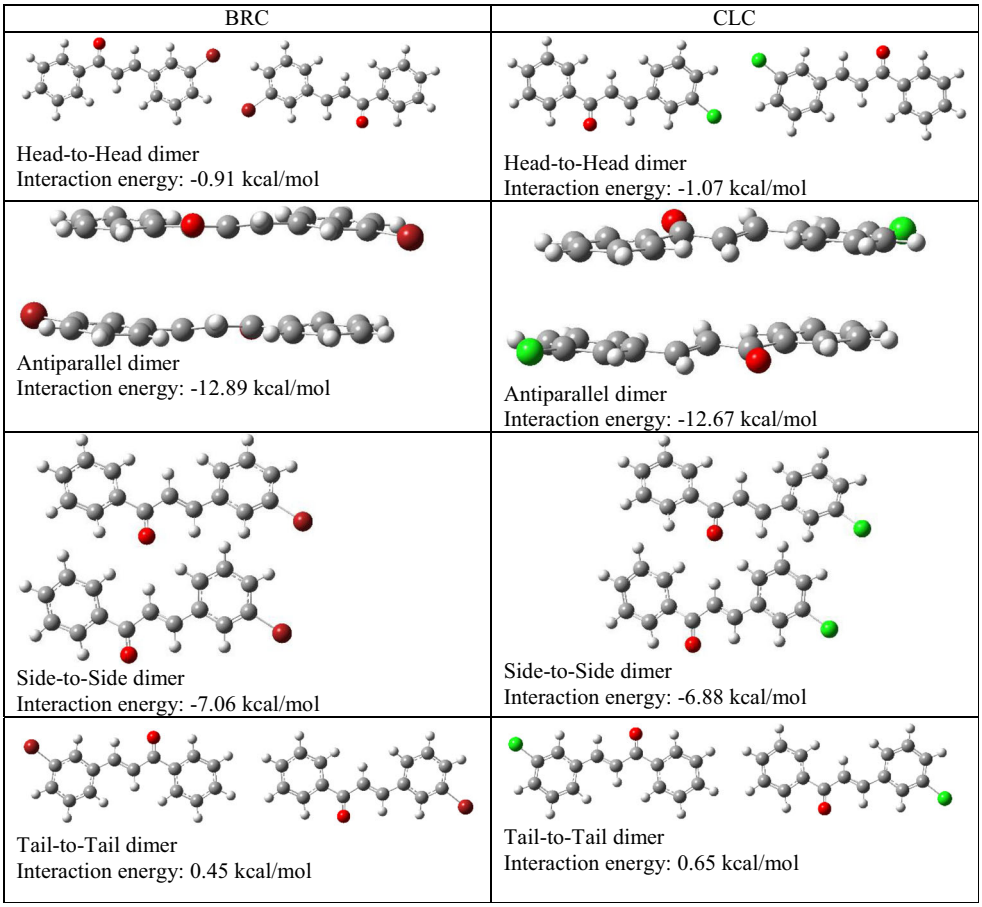

Fig. 14 Complexation energies obtained at M06-2X/6-311++G(d,p) level of theory. The heavy atom coordinates were taken from X-ray data, and the hydrogen atoms were optimized at the same level of theory. The basis set superposition errors were corrected using the counterpoise procedure

interaction in the CLC molecule and Fig. 13b shows the equivalent interaction of this in the BRC molecule (C4–H3…Cg1). The interactions C–H...Cg2 are shown in Figs. 13c for the molecule CLC (C15–H15...Cg2) and 13d for the molecule BRC (C1–H1...Cg2).

Theoretical analysis and isostructures

With the aim of explaining the experimental observations in which both structures, BRC and CLC have the same crystallographic parameters; quantum mechanics calculations were carried out at the M06-2X/6-311++G(d,p) [34] level of the theory for both compounds. The atom coordinates used as input in the calculations were taken from the X-ray data, and only the hydrogen atom geometric parameters were optimized for each dimer. Figure 14 shows that there are four types of interaction for each molecule in the solid-state, which we call here the head-to-head, antiparallel, side-to-side, and tail-to-tail dimers. The basis set superposition errors (BSSE) for the interaction energies were corrected using the counterpoise [35, 36] procedure implemented in the g16 program.

Figure 14 shows that the head-to-head interaction energies for both BRC and CLC dimers are − 0.91 kcal/mole and − 1.07 kcal/mole, respectively. It is worth noting that the

Table 3 Topological parameters of chalcones describing contacts and intermolecular interactions (electron density at BCP ($\rho(\mathbf{r})$), Laplacian ($\nabla^2\rho(\mathbf{r})$), the potential electron energy density ($V(\mathbf{r})$). All values are given in atomic units (au)

BCP	Types	$\rho(\mathbf{r})^a$	$\nabla^2\rho(\mathbf{r})^a$	$V(\mathbf{r})^a$
1	C13–H13···Cl1	0.01409	0.04169	− 0.00582
2	C13–H13···Cl1	0.02071	0.04934	− 0.00895
3	C13–H13···Br1	0.01488	0.03061	− 0.00765
4	C13–H13···Br1	0.01492	0.03908	− 0.00865
5	C5–H5···O1	0.04417	0.06580	− 0.02203
6	C8–H8···O1	0.04500	0.08020	− 0.02378
7	C11–H11···O1	0.07774	0.09789	− 0.05783
8	C5–H5···O1	0.05173	0.06476	− 0.02497
9	C8–H8···O1	0.03796	0.05125	− 0.02221
10	C11–H11···O1	0.03604	0.06036	− 0.02555
11	C2–H2···H3–C3	0.02328	0.08186	− 0.01996
12	C3–H3···H2–C2	0.04913	0.16120	− 0.03174
13	C2–H2···H3–C3	0.03035	0.12910	− 0.01979
14	C3–H3···H2–C2	0.04280	− 0.0058	− 0.01500
15	π ···π	0.04856	0.01207	− 0.01315
16	π ···π	0.05431	0.04038	− 0.01614
17	π ···π	0.04480	0.02034	− 0.01232
18	π ···π	0.03758	0.02956	− 0.01098

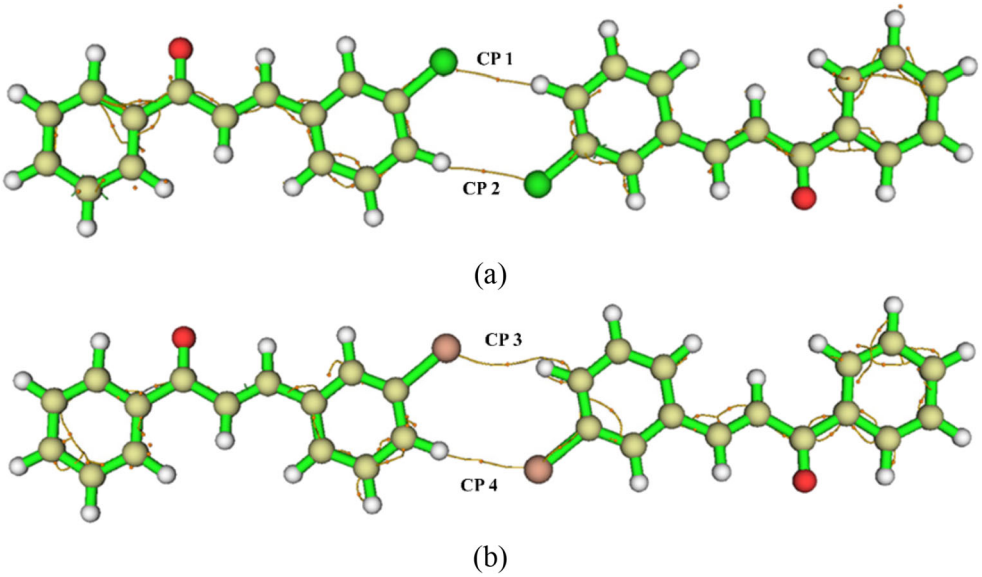

Fig. 15 The molecular graphs, head-to-head interaction, showing the bond critical points (BCP) in yellow, **a** in CLC, **b** in BRC

interaction energies are small and similar for both dimers. These results are interesting because we replaced the chlorine atom with a bromine atom that has 18 more electrons, and the interaction energies did not change much. Furthermore, the interaction energies for BRC and CLC antiparallel dimers are − 12.89 kcal/mole and − 12.67 kcal/mole.

On the other hand, the antiparallel interaction energy is about 14 times greater than head-to-head for BRC and about 12 times greater for CLC. The side-to-side dimer interaction energies are also powerful. These are about 8 times greater than head-to-head dimer interaction energy for BRC and about 6 times greater for CLC. The tail-to-tail interaction energies are small and repulsive for both dimers. Based on the interaction energies for the different dimers found in the solid-state, we can postulate that the side-to-side and the antiparallel interactions are the interaction forces that drive the crystal growth. In this sense, the head-to-head interaction, where chlorine replaces bromine, is not energetically significant in the crystal growth process, which explains the fact that the two compounds show the same crystallographic parameters.

In order to better understand the nature of the dimer interactions energies, the QTAIM analysis was employed as a powerful tool to study the nature of intermolecular interactions. According to Boyd et al (2007) [63], the interactions with $\rho(\boldsymbol{r}) > 0.2$ a.u. and $\nabla^2\boldsymbol{\rho}(\boldsymbol{r}) < 0$ at the bond critical point (BCP) are predominantly covalent, and those with $\rho(\boldsymbol{r}) < 0.1$ a.u. and $\nabla^2\boldsymbol{\rho}(\boldsymbol{r}) > 0$ at BCP are classified as closed-shell interactions such as hydrogen bonds, van der Waals interactions, and ionic bonds.

Figures 15, 16, 17, and 18 show the BCP in yellow. Table 3 shows that the electro density ($\rho(\boldsymbol{r})$) at BCP is less than 0.1 a.u. and the Laplacian ($\nabla^2\boldsymbol{\rho}(\boldsymbol{r})$) values for all BCP are positive, except for BCP 16 that has a negative value. However, the Laplacian value for BCP 16 is remarkably close to zero. From the QTAM analysis, we can conclude that the interactions for all dimers can be classified as van der Waals or closed-shell interactions.

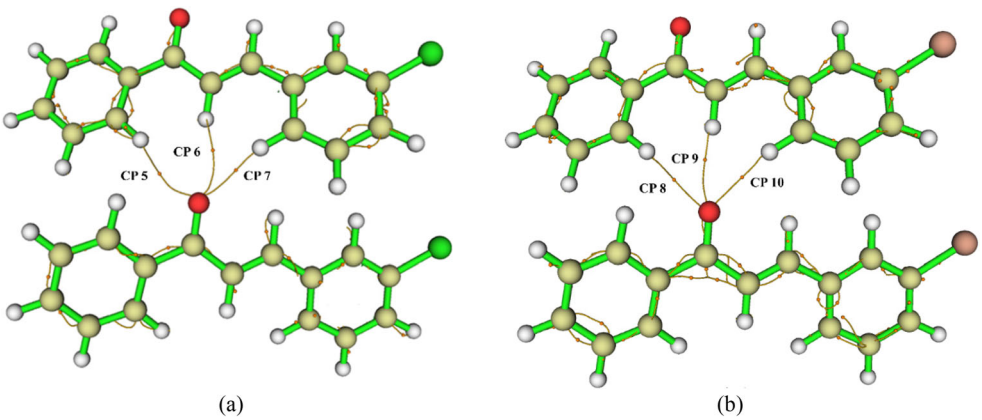

Fig. 16 The molecular graphs, side-to-side interaction, showing the bond critical points (BCP) in yellow, **a** in CLC, **b** in BRC

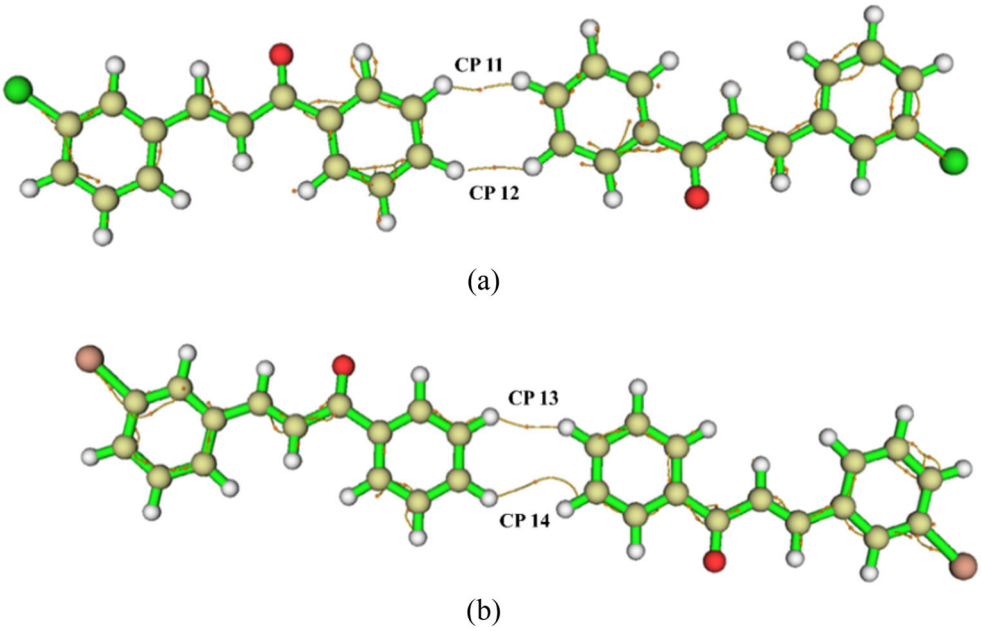

Fig. 17 The molecular graphs, tail-to-tail interaction, showing the bond critical points (BCP) in yellow, **a** in CLC, **b** in BRC

Supermolecule scheme analysis

The NLO properties of crystals CLC and BRC were obtained from the SM model using the functional DFT/CAM-B3LYP together with the base function 6-311++G(d,p) and discussed as a function of the applied electric field frequency. Table 4 shows the increase in average linear polarizability $\langle\alpha(-\omega,\omega)\rangle$of crystals CLC and BRC. When the frequency goes from the static case (ω = 0) to the dynamic case (ω = 0.1 a.u.), we can see an increase of 18.37% for compound CLC and 19.13% for compound BRC. The average second hyperpolarizability IDRI $\langle\gamma(-\omega;\omega,\omega,-\omega)\rangle$ of crystals CLC and BRC showed an increase of 382.39% and

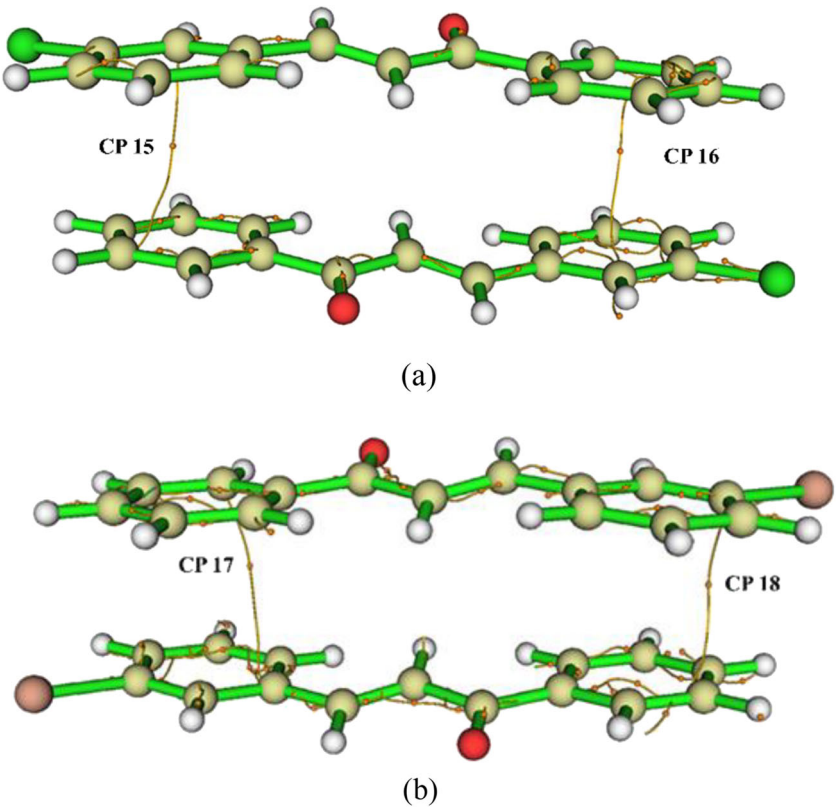

Fig. 18 The molecular graphs, antiparallel interaction, showing the bond critical points (BCP) in yellow, **a** in CLC, **b** in BRC

Table 4 Results of linear polarizability $\langle\alpha(-\omega,\omega)\rangle$, second average hyperpolarizability IDRI $\langle\gamma(-\omega;\omega,\omega,-\omega)\rangle$, of the compounds CLC and BRC using the SM approach

	CLC	BRC	CLC	BRC
ω	$\langle\alpha(-\omega,\omega)\rangle$	$\langle\alpha(-\omega,\omega)\rangle$	$\langle\gamma(-\omega;\omega,\omega,-\omega)\rangle$	$\langle\gamma(-\omega;\omega,\omega,-\omega)\rangle$
0.000	28.439	30.084	54.241	60.372
0.003	28.442	30.087	54.608	60.861
0.004	28.444	30.090	54.667	60.928
0.006	28.452	30.098	54.835	61.118
0.007	28.456	30.103	54.945	61.243
0.008	28.462	30.109	55.072	61.386
0.009	28.468	30.116	55.216	61.549
0.010	28.475	30.123	55.377	61.732
0.024	28.649	30.313	59.510	66.418
0.043	29.141	30.850	71.980	80.599
0.050	29.416	31.151	79.514	89.194
0.060	29.897	31.677	93.708	105.446
0.070	30.515	32.354	113.967	128.768
0.072	30.657	32.511	119.000	134.584
0.080	31.304	33.222	143.582	163.118
0.086	31.846	33.821	166.553	189.966
0.090	32.323	34.348	188.675	215.982
0.095	32.945	35.038	220.475	253.646
0.100	33.664	35.838	261.653	302.856

401.64%, respectively, when the comparison concerns the frequency range $\omega = 0$ to $\omega = 0.1$ a.u., as displayed in Table 4.

The analysis of electric charge transfer can be used to explain one of the causes for the nonlinear optical properties of compound BRC to be better than compound CLC. In Fig. 19, we highlight the rings A, B, and C and the details are shown in Table 5. Ring A shows a positive electric charge increase of 131.23% over the isolated structure of compound CLC, whereas in compound BRC, this increase is 177.97%. On the other hand, when analyzing ring B, we noticed a 36.73% increase in negative electric charge when the analysis was made between the isolated and embedded structures of compound CLC. Meanwhile, for the same ring B in BRC compound, the increase of negative electric charge is 38.93% between the isolated and embedded structures. In the case of ring C, we have an increase of positive electric charge of 24.04% for compound CLC and 32.40% for compound BRC when we compare the isolated structure with the involved one.

In both compounds, we have the following structure D-A-D: electron donor-acceptor-donor. The chlorine and bromine isostructures have an increase in electric charge transfers of 24.43% and 38.06%, respectively (when we look at the isolated and embedded structure). This change caused by the exchange of chlorine for bromine improves the nonlinear optical properties of the BRC compound.

Sum-over-states scheme

Figure 20 shows the results of the second static and dynamic average hyperpolarizability (λ=532 nm) for the isolated BRC and CLC molecules as a function of the number of excited states, using the SOS method. Considering the BRC compound, the value of the static second hyperpolarizability using this same method $\langle\gamma(0;0,0,0)\rangle_{SOS}$ is $-37.7\times10^{-36}esu$ while using the SM method, the value of $\langle\gamma(0;0,0,0)\rangle_{SM}$ is $60.372\times10^{-36}esu$, showing that the SM method is 1.6 times greater than SOS one (considering only values in module). Next, when we compare the average second hyperpolarizability IDRI of the BRC compound, we find that $\langle\gamma(-\omega;\omega,\omega,-\omega)\rangle_{SOS}$ is $49{,}969\times10^{-36}esu$ while the value of $\langle\gamma(-\omega;\omega,\omega,-\omega)\rangle_{SM}$ is $189.97\times10^{-36}esu$, showing that the SOS method is 263.04 times greater than the SM one. In the case of the CLC compound, the value of the second static hyperpolarizability $\langle\gamma(0;0,0,0)\rangle_{SOS}$ is $-19.11\times10^{-36}esu$ and $\langle\gamma(0;0,0,0)\rangle_{SM}$ is $54.24\times10^{-36}esu$ and for the case of average second hyperpolarizability IDRI, the values of $\langle\gamma(-\omega;\omega,\omega,-\omega)\rangle_{SOS}$ are $8{,}478.32\times10^{-36}esu$ whereas for $\langle\gamma(-\omega;\omega,\omega,-\omega)\rangle_{SM}$ is $166.55\times10^{-36}esu$, showing that the SOS method furnishes values 50.90 times greater than those using the SM method for $\langle\gamma(-\omega;\omega,\omega,-\omega)\rangle$.

The greatest increases in hyperpolarizability observed in the results of SOS are consistent with previous studies [53, 54, 56] and, in the current study, may mean that in the crystalline phase the values are even greater, indicating that the non-linear properties BRC and CLC compounds are good for application in optical devices. The SOS method confirms that the BRC structure has better NLO properties than CLC.

Refractive index and third-order nonlinear susceptibility

The linear refractive index (n_0) of the CLC and BRC crystals shown in Table 6 obtained through the Equation 5 showed an increase of 11.35% for compound CLC and 12.46% for compound BRC when comparing the static case ($\omega = 0$) with the dynamic case ($\omega = 0.1$ au). According to Equation 10, we obtain the third-order macroscopic susceptibility $\chi^{(3)}(-\omega;\omega,\omega,-\omega)$; this susceptibility also increases with the frequency applied to both compounds, as shown in Table 6. The increase, when comparing the static ($\omega = 0$) and dynamic ($\omega = 0.1$ a.u.) cases of compounds CLC and BRC, was 382.39% for CLC and 401.65% for BRC, coinciding with the result obtained for the average second hyperpolarizability IDRI.

Table 7 shows the linear refractive index (n_0) and the third-order macroscopic susceptibility of CLC and BRC crystals and other structures already studied in the literature. The results show that the property values displayed by CLC and

Table 5 Partial charges in isolated and embedded molecules of CLC and BRC

	CLC				BRC			
	Atom	Isolated	Embedded	Δ%	Atom	Isolated	Embedded	Δ%
1	Cl1	− 0.1549	− 0.1928	24.43	Br1	− 0.1059	− 0.1461	38.06
2	O1	− 0.5389	− 0.6127	13.69	O1	− 0.5409	− 0.6171	14.09
3	C1	− 0.0339	− 0.0368	8.65	C1	− 0.0407	− 0.0464	13.92
4	H1	0.0958	0.0821	14.29	H1	0.0986	0.0870	11.75
5	C2	− 0.1134	− 0.1326	16.88	C2	− 0.1098	− 0.1248	13.60
6	H2	0.1045	0.1080	3.36	H2	0.1038	0.1062	2.31
7	C3	− 0.0682	− 0.0347	49.12	C3	− 0.0693	− 0.0404	41.68
8	H3	0.0960	0.0972	1.21	H3	0.0942	0.0942	0.04
9	C4	− 0.0805	− 0.0929	15.42	C4	− 0.0831	− 0.0914	9.96
10	H4	0.0939	0.0996	6.12	H4	0.0932	0.0965	3.51
11	C5	− 0.1531	− 0.1647	7.57	C5	− 0.1392	− 0.1517	9.00
12	H5	0.1255	0.1629	29.82	H5	0.1174	0.1562	33.07
13	C6	− 0.0580	− 0.0682	17.65	C6	− 0.0581	− 0.0659	13.43
14	C7	0.5664	0.6178	9.08	C7	0.5624	0.6134	9.06
15	C8	− 0.3039	− 0.3128	2.94	C8	− 0.3201	− 0.3300	3.10
16	H8	0.1176	0.1191	1.34	H8	0.1302	0.1322	1.54
17	C9	− 0.0331	− 0.0254	23.33	C9	− 0.0251	− 0.0154	38.76
18	H9	0.1240	0.1211	2.35	H9	0.1283	0.1264	1.49
19	C10	0.1211	0.1396	15.32	C10	0.1200	0.1376	14.63
20	C11	− 0.1818	− 0.2121	16.67	C11	− 0.1972	− 0.2232	13.15
21	H11	0.1439	0.2042	41.92	H11	0.1476	0.2062	39.67
22	C12	− 0.1148	− 0.1252	9.06	C12	− 0.0841	− 0.0943	12.13
23	H12	0.1205	0.1200	0.37	H12	0.1120	0.1119	0.06
24	C13	− 0.0664	− 0.0696	4.81	C13	− 0.0776	− 0.0868	11.98
25	H13	0.1034	0.1147	10.96	H13	0.0945	0.1074	13.55
26	C14	0.1177	0.1537	30.56	C14	0.0742	0.1198	61.45
27	C15	− 0.1611	− 0.1868	15.93	C15	− 0.1315	− 0.1633	24.18
28	H15	0.1320	0.1273	3.52	H15	0.1059	0.1018	3.91
	Ring A	0.0086	0.0199	131.23	Ring C	0.0070	0.0196	177.97
	Ring B	− 0.0678	− 0.0928	36.73	Ring B	− 0.0652	− 0.0905	38.93
	Ring C	0.2142	0.2657	24.04	Ring A	0.1640	0.2171	32.40

BRC compounds outperform all structures operating at 532 nm wavelength.

A comparison of the theoretical values of compounds CLC and BRC with the experimental values of other crystalline compounds, in Table 7, shows that the value obtained for the third-order nonlinear macroscopic susceptibility, ($\chi^{(3)}(-\omega;\omega,\omega,-\omega)$), for the 532 nm wavelength of the CLC and (BRC) crystals, resulted in a value that was 329 (404.96) times larger when compared to (2E)-1-(3-bromophenyl)-3-[4(methylsulfanyl)phenyl]prop-2-en-1-one [69] and 2.36 (2.91) times larger than crystal (2E)-3-(3-methylphenyl)-1-(4-nitrophenyl)prop-2-en-1-one [64]. The exchange of chlorine (Cl) for bromine (Br) improved third-order macroscopic susceptibility by 23.09% when analyzed at the wavelength 532 nm.

Conclusions

Both molecules crystallized in centrosymmetric space group $P2_1/c$ stabilized by the interactions C–H...O, C–H...Cl OR C–H...Br, C–H...π AND π ... π. Analysis of the HS showed that the interactions in the CLC and BRC molecules are the same as those observed in overlapping (Fig. 9). The head-to-head interaction energies, where chlorine is replaced by bromine, for both CLC and BRC dimers are − 1.07 kcal/mole and − 0.91 kcal/mole, respectively. Thus, it is not energetically significant in the crystal growth process, which explains the fact that the two compounds show the same crystallographic parameters. Also, the SM method associated with DFT/CAM-B3LYP/6-311++G(d,p) and sum-over-state method were used to calculate nonlinear electrical properties: second average

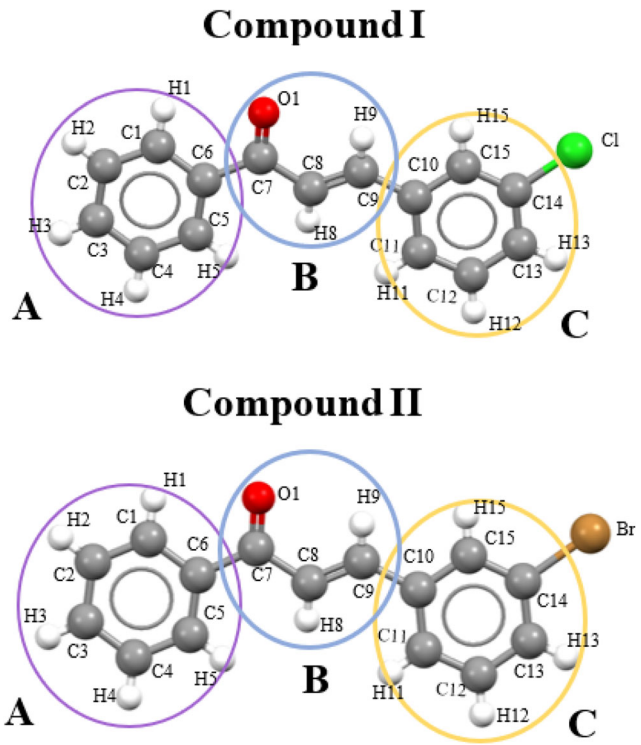

Fig. 19 Molecular structure of CLC and BRC with detached rings and numbered atoms

Table 6 Results of refractive index n_0, and third-order macroscopic susceptibility, $\chi^3(-\omega;\omega,\omega,-\omega)$, of the compounds CLC and BRC using the SM approach

	CLC	BRC	CLC	BRC
ω in a.u.	n_0	n_0	$\chi^{(3)}(-\omega;\omega,\omega,-\omega)$	$\chi^{(3)}(-\omega;\omega,\omega,-\omega)$
0.000	1.754	1.790	213.217	256.108
0.003	1.754	1.790	214.660	258.183
0.004	1.754	1.790	214.892	258.465
0.006	1.754	1.790	215.553	259.275
0.007	1.755	1.790	215.985	259.801
0.008	1.755	1.790	216.483	260.411
0.009	1.755	1.791	217.049	261.103
0.010	1.755	1.791	217.683	261.878
0.024	1.761	1.798	233.927	281.758
0.043	1.779	1.817	282.948	341.916
0.050	1.789	1.828	312.563	378.378
0.060	1.806	1.847	368.359	447.318
0.070	1.829	1.873	447.995	546.254
0.072	1.835	1.879	467.778	570.927
0.080	1.859	1.906	564.410	691.976
0.086	1.880	1.930	654.708	805.870
0.090	1.899	1.951	741.668	916.234
0.095	1.924	1.979	866.671	1076.011
0.100	1.953	2.013	1028.539	1284.769

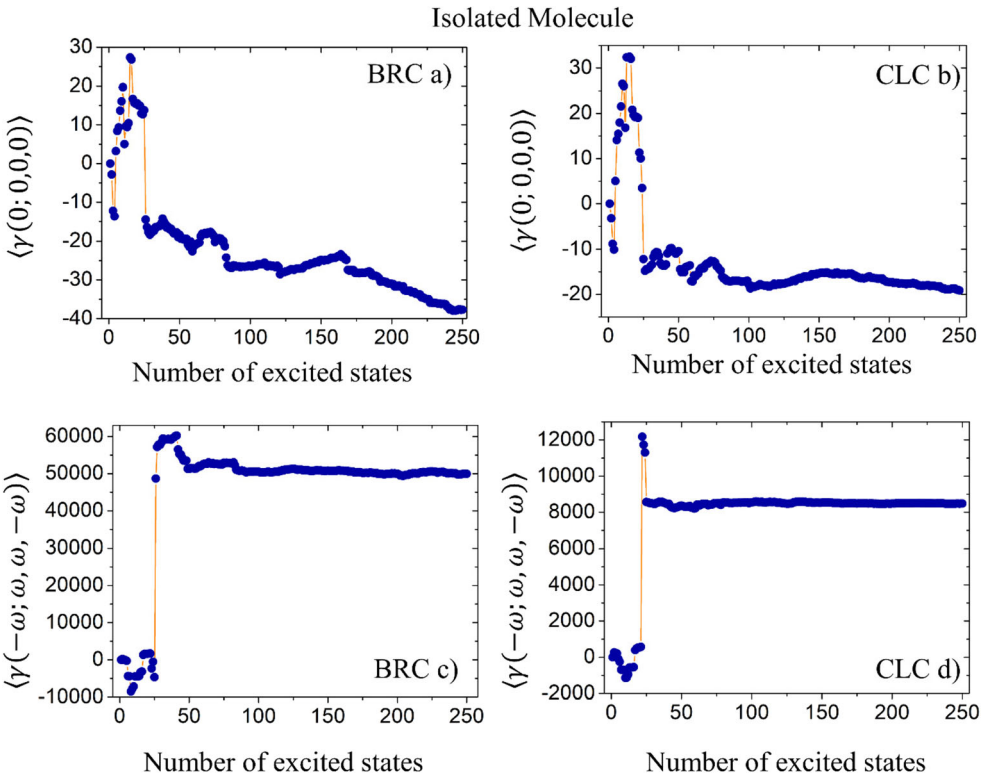

Fig. 20 $\langle\gamma(0;0,0,0)\rangle_{SOS}$ and $\langle\gamma(-\omega;\omega,\omega,-\omega)\rangle_{SOS}$ (λ=532 nm) calculated via SOS scheme, in units of 10^{-36}*esu*, for the BRC and CLC isolated molecules

Table 7 Comparison of results of the third-order nonlinear susceptibility $\chi^{(3)}\left(\times 10^{-22}\left(\frac{m}{V}\right)^2\right)$ for wavelength 532 nm using the SM approach

	n_0	$\chi^{(3)}(-\omega;\omega,\omega,-\omega)$
BRC (this work)	1.930	805.870
CLC (this work)	1.880	654.708
(2E)-3-(3-methylphenyl)-1-(4-nitrophenyl)prop-2-en-1-one [64]	1.418	277.100
4,6-dichloro-2-(methylsulfonyl)pyrimidine [41]	1.613	56.740
(E)-3-(2-bromophenyl)-1-(2-((phenylsulfonyl)amine)-phenyl)prop-2-en-1-one [40]	1.680	25.700
1-(5-chlorothiophen-2-yl)-3-(2,3-dimethoxyphenyl)prop-2-en-1-one [64, 65]	1.594	23.830
1-(5-chlorothiophen-2-yl)-3-(2,3-dichlorophenyl)prop-2-en-1-one [66]	-	16.210
2-(4-methylphenoxy)-N0-[(1E)-(4-nitrophenyl)methylene]acetohydrazide [67]	-	10.240
1-(4-aminophenyl)-3-(3,4,5-trimethoxyphenyl)prop-2-en-1-one [68]	-	8.700
(2E)-3 [4 (methylsulfanyl)phenyl]-1-(4-nitrophenyl)prop-2-en-1-one [69]	1.363	2.370
(2E)-1-(4-bromophenyl)-3-[4-methylsulfanyl phenyl]prop-2-en-1-one [69]	1.365	2.300
(2E)-1-(3-bromophenyl)-3-[4 (methylsulfanyl) phenyl]prop-2-en-1-one [69]	1.360	1.990

hyperpolarizability static $\langle\gamma(0;0,0,0)\rangle$ and IDRI $\langle\gamma(-\omega;\omega,\omega,-\omega)\rangle$ and including the calculations of the linear refractive index (n_0) and the third-order macroscopic susceptibility $\chi^3(-\omega;\omega,\omega,\omega)$ of two crystalline isostructures (CLC and BRC).

The difference between compounds CLC and BRC is the exchange of chlorine (CLC) for bromine (BRC); this exchange causes a 23.09% increase in the nonlinear third-order property of the Bromo compound. Both studied structures present better values in third-order macroscopic susceptibility than experimental results presented in the literature [39–41, 64–69]. The $\chi^{(3)}(-\omega;\omega,\omega,-\omega)$ of CLC exhibited an increase of 2.36 to 329 times greater than experimental results presented in the literature, while BRC showed an increase of 2.91 to 404.96. Therefore, isostructural crystals CLC and BRC are well suited for use as materials in applications involving NLO properties.

Acknowledgements The authors thank the High Performance Computing Center of the Universidade Estadual de Goiás (UEG). We also thank the organizers of the American Crystallographic Association 2019 Summer Course in Chemical Crystallography.

Author contribution Introduction: G.S. Ludovico, I.H.S. Barros, L.O. Sallum, R.S. Lima, C. Valverde, A.J. Camargo, B..Baseia, and H.B. Napolitano. Synthesis and crystallization: G.S. Ludovico and R.S. Lima. Crystallographic characterization: G.S. Ludovico, L.O. Sallum, and H.B. Napolitano. Theoretical and computational procedures: L.O. Sallum, A.J. Camargo, and H.B. Napolitano. Nonlinear optical properties: I.H.S. Barros, C. Valverde, and B..Baseia. Results and discussion: G.S. Ludovico, I.H.S. Barros, L.O. Sallum, R.S. Lima, C. Valverde, A.J. Camargo, B..Baseia, and H.B. Napolitano. Conclusions: G.S. Ludovico, I.H.S. Barros, L.O. Sallum, R.S. Lima, C. Valverde, A.J. Camargo, B. Baseia, and H.B. Napolitano.

Funding This research was funded by the Brazilian agencies Fundação de Amparo à Pesquisa do Estado de Goiás (FAPEG), Conselho Nacional de Desenvolvimento Científico e Tecnológico (CNPq), and Coordenação de Aperfeiçoamento de Pessoal de Nível Superior (CAPES, Finance Code 001).

Data availability CCDC code 2019801 was available at Cambridge Crystallography Data Center.

Compliance with ethical standards

Competing interests The authors declare no competing interests.

References

1. Jumaah M, Kwong HC, Khairuddean M (2019) Crystal structure of (E) -3- (2-hydroxy-4-methyl-) research communications. Acta Cryst E75:1379–1382
2. Duarte VS, Custodio JMF, Oliveira GR, Napolitano HB (2019) Benzodioxol group driving supramolecular arrangement of two tri-methoxy chalcones onto B -secretase 1 enzyme active site. J Braz Chem Soc 30:1916–1926
3. Ianelli S, Nardelli M, Giordano C, Coppi L, Restelli A (1992) Enantiomerically pure α-haloketals: structure and conformation of (2'S ,4'R ,5'R)-dimethyl 2'-halo-1',2',3',4'-tetrahydrospiro[1,3-dioxolane-2,1'-naphthalene]-4,5-dicarboxylates (halo = Cl, Br, I). Acta Cryst C48:1722–1727
4. Abu N, Ho WY, Yeap SK, Akhtar MN, Abdullah MP, Omar AR, Alitheen NB (2013) The flavokawains: uprising medicinal chalcones. Cancer Cell Int 13:102
5. Won S-J et al (2005) Synthetic chalcones as potential anti-inflammatory and cancer chemopreventive agents. Eur J Med Chem 40:103–112
6. Nowakowska Z (2007) A review of anti-infective and anti-inflammatory chalcones. Eur J Med Chem 42:125–137
7. Vasquez-Martinez YA et al (2019) Antimicrobial, anti-inflammatory and anti-oxidant activities of polyoxygenated chalcones. J Braz Chem Soc 30:286–304
8. Sulpizio C, Roller A, Giester G, Rompel A (2016) Synthesis , structure , and antioxidant activity. Monatsh Chem Chem Mon. https://doi.org/10.1007/s00706-016-1812-9
9. Hsieh CT, Chang FR, Tsai YH, Wu YC, Hsieh TJ (2018) 2-Bromo-4'-methoxychalcone and 2-Iodo-4'-methoxychalcone Prevent Progression of Hyperglycemia and Obesity via 5'-Adenosine-

Monophosphate-Activated Protein Kinase in Diet-Induced Obese Mice. Int J Mol Sci 19:2763
10. Shrestha A, Shrestha A, Park P, Lee E (2019) Hydroxyl- and halogen-containing chalcones for the inhibition of LPS-stimulated ROS production in RAW 264.7 macrophages : design, synthesis and structure – activity relationship study. Bull Kor Chem Soc 40: 729–734
11. Zaini MF, Razak IA, Anis MZ (2019) Crystal structure , Hirshfeld surface analysis and DFT studies of (E) -1- (4-bromophenyl) -3- (3-fluoro- phenyl) prop-2-en-1-one research communications. Acta Cryst E75:58–63
12. Kamanina NV et al (2012) Polyimide-fullerene nanostructured materials for nonlinear optics and solar energy applications. J Mater Sci Mater Electron 23:1538–1542
13. Likhomanova SV, Kamanina NV (2016) COANP-fullerenes system for optical modulation. J Phys Conf Ser 741:012146
14. Lu L et al (2017) Few-layer bismuthene : sonochemical exfoliation , nonlinear optics and applications for ultrafast photonics with enhanced stability. Laser Photonics Rev. https://doi.org/10.1002/lpor.201700221
15. Salvi R et al (2018) Diagnosing lung cancer using etoposide microparticles labeled with Tc. Artif Cells Nanomed Biotechnol 46:341–345
16. Luo M et al (2018) M2B10O14F6 (M = Ca , Sr): The first two noncentrosymmetric alkaline-earth fluorooxoborates as the promising next- generation deep-ultraviolet nonlinear optical materials M 2 B 10 O 14 F 6 (M = Ca , Sr): the first two noncentrosymmetric alka- line-eart. J Am Chem Soc 140:3884–3887
17. Cui Q (2017) Nonlinear optical spectroscopy of two-dimensional materials Qiannan Cui. University of Kansas.
18. Shi G et al (2017) Finding the next deep-ultraviolet nonlinear optical material : NH4B4O6F. J Am Chem Soc 139:10645–10648
19. Castro AN et al (2016) Theoretical study on the third-order nonlinear optical properties and structural characterization of 3-Acetyl-6-Bromocoumarin. Chem Phys Lett 653:122–130
20. Kálmán A, Párkányi L, Argay G (1993) Classification of the isostructurality of organic molecules in the crystalline state. Acta Cryst B49:1039–1049
21. Sheia-Lin N, Patil PS, Razak IA, Fun H-K, Dharmaprakkash SM (2006) 3-(3-Bromophenyl)-1-phenylprop-2-en-1-one. Acta Cryst E62:893–895
22. Panepucci HC, Donoso JP, Tannus A, Becmann N, Bonagamba TJ (1985) Nuclear magnetic resonance tomography: new images of the body. Sci Today 4:46–56
23. Skoog DA, Holler FJ, Nieman TA (1998) Principles of instrumental analysis. Saunders College Pub 5
24. Sheldrick GM (2015) SHELXT – Integrated space-group and crystal- structure determination research papers. Acta Cryst A71: 3–8
25. Sheldrick GM (2015) Crystal structure refinement with SHELXL. Acta Crystallogr Sect C Struct Chem 71:3–8
26. Puschmann H, Bourhis LJ, Dolomanov OV, Gildea RJ, Howard JAK (2011) OLEX2 – a complete package for molecular crystallography. Acta Crystallogr Sect A Found Crystallogr 67:C593–C593
27. Macrae CF et al (2006) Mercury: visualization and analysis of crystal structures. J Appl Crystallogr 39:453–457
28. Tan SL, Jotani MM, Tiekink ERT (2019) Utilizing Hirshfeld surface calculations , non-covalent interaction (NCI) plots and the calculation of interaction energies in the analysis of molecular packing research communications. Acta Cryst E75:308–318
29. Martin AD et al (2015) Hirshfeld surface investigation of structure-directing interactions within dipicolinic acid derivatives. Cryst Growth Des 15:1697–1706
30. Spackman MA, Jayatilaka D (2009) Hirshfeld surface analysis. CrystEngComm 11:19–32
31. Spackman MA, Mckinnon JJ (2002) Fingerprinting intermolecular interactions in molecular crystals. CrystEngComm 4:378–392
32. Frisch MJ, Trucks GW, Schlegel HB, Scuseria GE, Robb MA, Cheeseman JR, Scalmani G, Barone V, Petersson GA, Nakatsuji H, Li X, Caricato M, Marenich AV, Bloino J, Janesko BG, Gomper DJG (2016) No Title. Gaussian 16, Revision B.01.
33. Sallum LO et al (2019) Structural studies on dihydropyrimidine derivatives as Mycobacterium tuberculosis coenzyme-A carboxylase inhibitors. Z Kristallogr Cryst Mater 234:657–669
34. Zhao Y, Truhlar DG (2008) The M06 suite of density functionals for main group thermochemistry, thermochemical kinetics, noncovalent interactions, excited states, and transition elements: two new functionals and systematic testing of four M06-class functionals and 12 other functionals. Theor Chem Accounts 120:215–241
35. Simon S, Duran M, Dannenberg JJ (1996) How does basis set superposition error change the potential surfaces for hydrogenbonded dimers. J Chem Phys 105:11024–11031
36. Boys SF, Bernardi F (1970) The calculation of small molecular interactions by the differences of separate total energies . Some procedures with reduced errors. Mol Phys 19:553–566
37. Grabowski SJ (2011) What is the covalency of hydrogen bonding ? Chem Rev 111:2597–2625
38. Lu T, Chen F (2012) Multiwfn : a multifunctional wavefunction analyzer. J Comput Chem 33:580–592
39. Valverde C, Osório FAP, Fonseca TL, Baseia B (2018) DFT study of third-order nonlinear susceptibility of a chalcone crystal. Chem Phys Lett 706:170–174
40. Custodio JMF et al (2019) Chalcone as potential nonlinear optical material: a combined theoretical, structural, and spectroscopic study. J Phys Chem C 123:5931–5941
41. Murthy PK et al (2019) An analysis of structural and spectroscopic signatures, the reactivity study of synthetized 4,6-dichloro-2-(methylsulfonyl)pyrimidine: A potential third-order nonlinear optical material. J Mol Struct 1186:263–275
42. Custodio JMF et al (2019) Using the supermolecule approach to predict the nonlinear optics potential of a novel asymmetric azine. J Phys Chem A 123:153–162
43. Fonseca TL, Sabino JR, Castro MA, Georg HC (2010) A theoretical investigation of electric properties of L-arginine phosphate monohydrate including environment polarization effects. J Chem Phys 133:144103
44. Santos OL, Fonseca TL, Sabino JR, Georg HC, Castro MA (2015) Polarization effects on the electric properties of urea and thiourea molecules in solid phase. J Chem Phys 143:234503
45. Senthil K, Kalainathan S, Kumar AR, Aravindan PG (2014) Investigation of synthesis, crystal structure and third-order NLO properties of a new stilbazolium derivative crystal: a promising material for nonlinear optical devices. RSC Adv 4:56112–56127
46. Kongsted J, Osted A, Mikkelsen KV, Christiansen O (2004) Second harmonic generation second hyperpolarizability of water calculated using the combined coupled cluster dielectric continuum or different molecular mechanics methods. J Chem Phys 120: 3787–3798
47. Kleinman DA (1962) Nonlinear dielectric polarization in optical media. Phys Rev 126:1977–1979
48. Bishop DM, De Kee DW (1996) The frequency dependence of nonlinear optical processes. J Chem Phys 104:9876–9887
49. Orr BJ, Ward JF (1971) Perturbation theory of the non-linear optical polarization of an isolated system. Mol Phys 20:513–526
50. Kuzyk MG (2005) Compact sum-over-states expression without dipolar terms for calculating nonlinear susceptibilities. Phys Rev A 72:053819
51. He Y-Y et al (2019) Spiral graphene nanoribbons with azulene defects as potential nonlinear optical materials. ACS Appl Nano Mater 2:1648–1654

52. Champagne B, Kirtman B (2006) Evaluation of alternative sum-over-states expressions for the first hyperpolarizability of push-pull π-conjugated systems. J Chem Phys 125:024101
53. Pérez-Moreno J, Clays K, Kuzyk MG (2008) A new dipole-free sum-over-states expression for the second hyperpolarizability. J Chem Phys 128:084109
54. Panja N, Ghanty TK, Nandi PK (2010) A sum-over-state scheme of analysis of hyperpolarizabilities and its application to spiroconjugated molecular system. Theor Chem Accounts 126: 323–337
55. Castet F et al (2013) Design and characterization of molecular nonlinear optical switches. Acc Chem Res 46:2656–2665
56. Coe JP, Paterson MJ (2014) Approaching exact hyperpolarizabilities via sum-over-states Monte Carlo configuration interaction. J Chem Phys 141:124118
57. Li W et al (2016) The structural and photophysical properties of multibranched derivatives with curved conjugated aromatic cores. J Mater Chem C 4:6054–6062
58. Tonnelé C, Champagne B, Muccioli L, Castet F (2018) Second-order nonlinear optical properties of Stenhouse photoswitches: insights from density functional theory. Phys Chem Chem Phys 20: 27658–27667
59. Rtibi E, Abderrabba M, Ayadi S, Champagne B (2019) Theoretical assessment of the second-order nonlinear optical responses of lindqvist-type organoimido polyoxometalates. Inorg Chem 58: 11210–11219
60. Gubler U, Bosshard C (2000) Optical third-harmonic generation of fused silica in gas atmosphere: absolute value of the third-order nonlinear optical susceptibility χ^(3). Phys Rev B 61:10702–10710
61. Frisch M et al (2009) Gaussian 09, revision D. 01.
62. Hathwar VR, Roopan SM, Subashini R, Khan FN, Row TNG (2010) Analysis of Cl … Cl and C – H … Cl intermolecular interactions involving chlorine in substituted 2-chloroquinoline derivatives. J Chem Sci 122:677–685
63. Boyd RJ, Matta CF (2007) The Quantum Theory of Atoms in Molecules.
64. Prabhu SR, Jayarama A, Chandrasekharan K, Upadhyaya V, Ng SW (2017) Synthesis, growth, structural characterization, Hirshfeld analysis and nonlinear optical studies of a methyl substituted chalcone. J Mol Struct 1136:244–252
65. Prabhu AN, Upadhyaya V, Jayarama A, Subrahmanya Bhat K (2013) Synthesis, growth and characterization of π conjugated organic nonlinear optical chalcone derivative. Mater Chem Phys 138: 179–185
66. Prabhu AN, Upadhyaya V, Jayarama A, Bhat KS (2016) Third-order NLO property of thienyl chalcone derivative: physicochemical analysis and crystal structure determination. Mol Cryst Liq Cryst 637:76–86
67. Naseema K et al (2010) Synthesis, characterization and studies on the nonlinear optical parameters of hydrazones. Opt Laser Technol 42:741–748
68. Ravindra HJ, Chandrashekaran K, Harrison WTA, Dharmaprakash SM (2009) Structure and NLO property relationship in a novel chalcone co-crystal. Appl Phys B Lasers Opt 94:503–511
69. D'silva ED, Podagatlapalli GK, Venugopal Rao S, Dharmaprakash SM (2012) Study on third-order nonlinear optical properties of 4-methylsulfanyl chalcone derivatives using picosecond pulses. Mater Res Bull 47:3552–3557